Acta Astronautica 140 (2017) 517–536

Contents lists available at ScienceDirect

Acta Astronautica

journal homepage: www.elsevier.com/locate/actaastro

A structural assessment of unrefined sintered lunar regolith simulant

Stephen J. Indyk [a,*], Haym Benaroya [b]

[a] Honeybee Robotics, 398 W. Washington Blvd. Suite 200., Pasadena, CA 91101, USA
[b] Department of Mechanical and Aerospace Engineering, Rutgers University, 98 Brett Rd, Piscataway, NJ 08854, USA

ARTICLE INFO

Keywords:
Lunar in-situ-resource utilization
Structural in-situ-resource utilization
Lunar regolith
In-situ resource utilization (ISRU)

ABSTRACT

The potential of utilizing lunar regolith as the raw material for manufacturing structural members is very appealing for future exploration and settlement of the Moon. Future lunar missions will depend on in-situ resource utilization (ISRU) for structural components, among other things. Sintered lunar regolith has been proposed as a structural material. In general, it has been assumed that the regolith would be at least minimally processed before use. We propose the possibility of manufacturing structural components directly using unrefined sintered lunar regolith with the advantage of requiring fewer specialized material processing equipment.

Our purpose in this study was the quantification of the material properties of unrefined sintered lunar regolith simulant. Two batches of sintered lunar regolith simulant JSC-1A samples, with porosities of 1.44% and 11.78%, underwent compression testing using an Instron series 4500 Universal Test System machine. Material properties were evaluated from the acquired load vs. deflection data. Stress vs. strain, modulus of elasticity, toughness, bulk modulus and compressive strength were evaluated as a function of porosity. The average compressive strength of the 1.44% porosity material was 218.8 MPa, and 84.6 MPa for the 11.78% porosity material. Our tests show that even unrefined sintered 11.78% porosity lunar regolith holds the possibility of being a useful structural material for lunar construction. Comparing our experimental results with those of other ISRU derived structural materials, unrefined sintered lunar regolith is expected to be one of the strongest material derived from lunar sources.

1. Introduction

From the log cabins built from trees felled by settlers of the American Pacific Northwest to the reinforced concrete, steel and glass skyscrapers towering over Manhattan and other modern cities, humans have been constructing progressively more complex structures. The lime and clay processed into cement and the iron ore forged into steel share the same humble beginnings as the timber harvested by logging - they originated from Earth. Making use of indigenous materials to construct dwellings has been a human activity for millennia. Of course, human-inhabited structures are simply a convenient example of what has and can be constructed from indigenous materials. Structural materials comprise a majority of man-made objects, such as underground pipes, smart phone housings, aircraft fuselages and many more. They all share a thread of being constructed from indigenous, processed and, of course, refined materials. Determining the strength and capabilities of structures depends heavily on the material used to create the structure, as well as the application envisioned. Through testing and statistical analysis, the strength of materials has become a fundamental field. With information available about common materials only a click away on the Internet, and with finite element analysis (FEA) software readily available, the real difficulty in assessing structural materials becomes apparent when investigating new materials.

Colonizing the Moon has been a human dream since mankind first looked up at the night sky. Before any such dream can become a long-term reality, it is necessary to first learn how to use existing lunar resources. However, the difficult environment of the Moon does not afford its first settlers the luxury of simply chopping down trees to construct shelter. Instead, these intrepid settlers will have to rely on constructed habitats transported from Earth for a considerable period of time. These domiciles will be well thought out, having exact placements on the lunar surface decided well in advance by Moon surveying satellites in order to maximize, or minimize, the effects of the Sun, ensure constant communication with Earth and allow spacecraft to ferry goods to and from this home away from home. Later, second or third generation lunar structures will be constructed mostly, if not entirely, out of indigenous materials.

The potential utilization of lunar regolith as a raw material for manufacturing structural members is very promising for future

Abbreviation: SLS, Sintered lunar simulant.

* Corresponding author.
E-mail addresses: indyk@honeybeerobotics.com (S.J. Indyk), benaroya@soe.rutgers.edu (H. Benaroya).

https://doi.org/10.1016/j.actaastro.2017.09.018
Received 14 April 2017; Received in revised form 2 August 2017; Accepted 18 September 2017
Available online 20 September 2017
0094-5765/© 2017 IAA. Published by Elsevier Ltd. All rights reserved.

exploration and settlement. For economic and practical reasons, future lunar missions will eventually depend on in-situ resource utilization (ISRU) for lunar structural components. Manufacturing structural components directly from unrefined lunar regolith would advantageously require less specialized terrestrial equipment. One method to forge structural material from unrefined lunar regolith is a process known as sintering. A possible issue with sintering from a structural perspective is the pores created in the sintering process. 'The more vacuum a thing contains within it, the more readily it yields …,' words written in the first century B.C. by the Roman philosopher Lucretius in his work entitled, *On the Nature of the Universe*. That porosity affects material strength is not a new concept.

We address the question of how processed does the lunar regolith have to be in order to consider it of structural quality.

1.1. Research goals

In order to further explore and develop the Moon, long-duration surface missions will increasingly depend on ISRU. Otherwise, everything necessary for building habitable structures on the Moon would have to be transported from Earth, which is economically unsustainable. Fortunately, the Moon itself provides a promising and easily accessible raw material via its regolith that may be used to construct habitats and other structures. Lunar regolith is a granular substance that is not only plentiful on the Moon, but can also be easily extracted and sintered for use in large load bearing structures.

From a structural perspective, it is expected that lunar settlement would take place in three phases: the first phase would require prefabricated structures to be transported from Earth to the Moon. Phase two would comprise of hybrid structures, partially terrestrially built, and finalized on the lunar surface. Finally, the third phase would see structures that are primarily composed of lunar-derived structural material. Thus, it is important to develop a path to increase the maturity of the technologies needed to manufacture, inspect and construct these indigenous lunar structures.

Several types of lunar regolith-derived structural materials have been previously proposed and studied, some more thoroughly than others. Each depends on various methods for working with the lunar regolith. Some methods refine the lunar regolith into raw ore, where others form more conventional construction materials by combining regolith with additives to produce lunar concrete. The practicality of these materials have been extensively evaluated to the point that elastic material constants are understood, see works such as Lin [1] and Toutanji et al. [2]. Oppositely, qualitative evaluations of the structural potential of sintered lunar regolith have been studied to a lesser extent. Sintering, the process of applying heat to a powder compact to increase strength and integrity, has previously been shown by researchers such as Taylor and Meek [3] to be a possible method of converting raw lunar regolith to solid components. However, the sintering process itself contains many variables to control, the foremost being porosity. Porosity significantly affects strength as well as other properties of sintered materials.

A central aspect of this work is to determine whether unrefined sintered lunar regolith is a viable lunar ISRU structural material, and which parameters are of most impact. Developing an understanding of how porosity affects the elastic material constants of unrefined sintered lunar regolith is our goal. To this end, we investigate the properties of high and 1.44% porosity lunar simulant.

The effects of porosity on basic material properties, such as bulk modulus, Young's modulus, toughness and compressive strength, were investigated. Compression testing of the sintered lunar simulant was performed, and then stress and strain values were computed from recorded load and deflection data. These collected material properties were also compared with similar terrestrial materials. The data were also compared to other potential lunar ISRU derived materials.

Our overarching motivation has been whether structures can be constructed on the Moon using unrefined sintered lunar regolith. Our primary contribution is the examination of sintered lunar regolith properties via experiments and our assessment of that data. The short answer is: yes, it will be possible to erect surface lunar structures using unrefined sintered lunar regolith.

1.2. The lunar environment

An understanding of the lunar environment is prerequisite to the design of any system that is expected to operate on the Moon. Based on the *Lunar Sourcebook* by Heiken et al. [4] we summarize some key lunar environmental parameters. The Moon is Earth's nearest celestial body at an average distance of 284,400 km. The lunar gravitational constant is 1.622 m/s^2 whereas Earth's gravitational constant is 9.81 m/s^2, making lunar gravity approximately 1/6th that of the Earth. Lunar regolith is abundant and coats the surface of the Moon. Median depths of the lunar regolith have been estimated to be 2–4 m in the mare regions and 6–8 m on the far side and non-mare nearside areas. The increase in density with depth leads to significant difficulties in excavation. The dust environment is another engineering concern.

Regolith is very fine grained, and its mean grain size ranges from 40 to 900 μm with most mean values being between 45 and 100 μm. Particles below 20 μm in size have also been found. Materially, regolith contains heavy metals with many minerals common to those on Earth. This includes hard rocks and minerals such as basalt, anorthosite and olivine. Once disturbed, the regolith is electrostatically charged and can remain suspended 1–2 m above the surface for long periods of time. All of these properties make the regolith a serious threat to any mechanical system, leading to accelerated wear due to the regolith's abrasiveness. It is also considered to be a carcinogenic threat.

The lunar surface has low thermal capacity and very low thermal conductivity, making heat retention difficult. Surface temperatures between 374 and 92 K have been measured at the Apollo 15 landing site. Intense solar radiation exists at the lunar surface with intensities of between 1316 W/m^2 and 1421 W/m^2, depending on the position of the Earth relative to the Sun. For comparison, radiation at the Earth's surface is about 0.095 W/m^2. The lunar surface has a high vacuum with a pressure of 2.667e-13 kPa (2e-12 Torr) at night. For comparison, average sea-level pressure on the Earth's surface is 101.325 kPa (760 Torr).

1.3. Literature review

There are four main reasons why sintering lunar regolith is an efficient and viable option for use as a structural material. First, there is a need for ISRU. Secondly, there are limited alternative materials that could be made from ISRU without extensive refinement. Third, the current state of manufacturing process technology available would allow for effective sintering manufacturing. And finally, there are a multitude of useful structures that could be produced with sintered lunar regolith. Relevant research work is listed below and evaluated on these four criteria. Our research is focused on sintering of unprocessed lunar regolith.

Our review of the literature is organized based on relevance to this research effort. Special attention is given to experiments that estimate material properties. Relevance is based on four fundamental classifications; the need for ISRU, alternative ISRU materials, manufacturing processes, and what could be constructed.

1.3.1. The need for ISRU

Duke et al. [5] developed a strategy for exploration and development of the Moon. A main focus was the economics of going to the Moon. The cost of transporting material from the Earth into orbit was cited as a main problem with commercializing space. Development of the Moon would allow for natural resource access and a space transportation infrastructure. ISRU was discussed as a key factor in the development of the Moon. Resources that could come directly from the Moon included power, propellants, life support consumables and structural materials. Sintering

regolith, cast basalt, concrete and microwave processing of regolith were discussed as potential structural materials. Benaroya et al. [6–8] provides an extensive review of ISRU.

1.3.2. Alternative materials from ISRU

There have been investigations into utilizing the lunar regolith to make concrete. Testing of both actual lunar regolith and lunar simulant has been conducted, resulting in compressive strength measurements. Two works of note involve actual lunar material, and an additive laden lunar concrete.

Researchers led by Lin [1] created lunar concrete using 40 g of a sample of regolith. The sample was acquired by Apollo 16, and is from the lunar mare, the large dark basaltic plains on the Moon formed by ancient volcanic activity. Testing of the samples found a compressive strength of 74 MPa (10,000 psi), a tensile strength of 8.3 MPa (1200 psi), a modulus of elasticity of 21,400 MPa (3.1×10^6 psi) and a thermal expansion coefficient of 5.4×10^{-6} cm/cm/°C (2.9×10^{-6} in/in/°F).

Toutanji et al. [2] created cast blocks of lunar concrete using JSC-1 mixed with sulfur powder in a 65%–35% ratio and measured a 31 MPa compressive strength. Sulfur, previously shown to be on the Moon, is another viable ISRU option for lunar concrete.

Landis [9] developed refining processes that could produce several heavy metals from lunar ISRU. Aluminum, iron, calcium and magnesium were among those elements that could be reacted with fluorine. Material properties of these metals would be expected to be the same as those on Earth and depend on the quality of the refining and material processing.

Benaroya et al. [10] specifically advocated the use of magnesium as an ISRU derived structural material. High strength to weight ratio, high impact resistance and vibration damping 30 times that of aluminum were cited as favorable characteristics for refining magnesium for use in structures.

In addition to cements and metals, utilizing the raw lunar regolith, with or without additives, has also been proposed as structural materials. Specific manufacturing processes have been suggested and are discussed next.

1.3.3. Manufacturing processes

Several novel means of manufacturing materials derived from lunar sources have been researched and tested. Processes involving additive manufacturing, casting, microwaving and thermite reactions have been investigated previously.

Allen et al. [11] demonstrated the possibility of producing cast-sintered bricks of lunar simulant. Using radiant heating, microwave heating, and a combination of both, cast brick-sized blocks of sintered lunar simulant were created. The main purpose of this work was to develop practical methods of sintering to produce lunar bricks. Two simulants were used in their tests, MLS-1 and the venerable JSC-1. A recommended sintering temperature of 1100 °C was found to be the most effective to produce solid bricks. Since quality was of main concern, sintering behavior is significantly improved by compaction of the simulant. This is because of a decrease in porosity and an increase of grain-to-grain contact. Incorporating vibratory compacting into the manufacturing process was also suggested. Since crushed rock is effectively an insulator, thermal cracking could be an issue. Thermal cracking could be minimized by allowing for relatively long heating and cooling periods. During some of their manufacturing tests, the bricks were stuck to the mold and had to be chipped out. Difficulties of casting large blocks of sintered lunar simulant were acknowledged and it should be expected that actual lunar regolith would behave similarly. Different environments for sintering were also used, for example, conducting sintering in argon and hydrogen atmospheres, but not in a vacuum.

While this research excelled in manufacturing process development, it stopped short of performing material property investigations. Testing was conducted under atmospheric conditions while it is expected that manufacturing on the Moon would lead to better quality material by using vacuum sintering. The operational use of molds to form blocks yields some concerns with the limits on the size of the molds and whether they should be fabricated on site or transported from Earth.

Microwave sintering was investigated utilizing actual lunar regolith. Taylor and Meek [3] showed that one critical property was the presence of native nanophase Fe^0, which was formed as a result the auto-reduction of the FeO in the silicate melts formed by micrometeorite impacts. Since nanophase Fe^0 was caused by meteoritic impacts, the more mature the lunar soil, the higher the nanophase Fe^0 concentration found. Nanophase Fe^0 are particles of iron with grain sizes less than 100 nm. Because of this iron inclusion, lunar regolith can be melted with a common household microwave in a matter of minutes. Microwaving allows the regolith to heat rapidly to temperatures of between 1200 °C and 1500 °C. No lunar simulants contained nanophase Fe^0 at the time of this study. Hence, this microwavability property of lunar regolith was not discovered earlier since so much work with lunar regolith was done using simulants, thus emphasizing the importance of working with actual lunar material.

Taylor and Meek [3] also suggested some applications of their discovery; microwave sintering could yield a smooth surface, one that could be used for producing an antenna dish or other surfaces that would benefit from a glass-like finish.

The exact manufacturing process is not discussed in this paper, making it difficult to quantitatively evaluate parameters such as rate of manufacture or energy consumption. Material excavation and post processing are required of any structural material fabricated by microwave sintered lunar regolith. Material properties were not investigated quantitatively, leaving an uncertainty in the quality of material produced from this process or its structural capacity. However, this research has created a demand for the investigation of this microwavability property further. Hung and McNatt [12] have been since able to file for a patent on the process of adding nanophase Fe^0 to lunar simulants.

Faierson et al. [13] studied a lunar structure constructed from ISRU resources. Structural components were fabricated using a geothermite reaction with a mixture of JSC-1AF and JSC-1A lunar simulants and aluminum powder. A geothermite reaction is one between minerals and a reducing agent exhibiting a thermite type of reaction behavior. In this case the minerals were the lunar simulant and the reducing agent was the aluminum powder. The process involves oxidation-reduction reactions between the constituents of the reactant mixture. Similar to casting, molds were used to form sintered blocks in a few carefully selected shapes. Once assembled, the blocks would form a voussoir dome. A voussoir is a wedge shaped element used in constructing an arch or vault, and a voussoir dome is a three dimensional surface comprised of these wedge shaped elements. Fabrication of the blocks was performed under standard terrestrial atmospheric conditions and used NiCr wire to initiate the reaction. Compression tests were conducted on samples of about 5 cm in height and about 2.5 cm in diameter. Experimental data indicated an ultimate strength range of 10–18 MPa depending on particle size and the ratio of aluminum to lunar simulant. For their calculations, a hypothetical value of 13.8 MPa was used. The dome shape was feasible and suggested an upper bound to the size of the dome possible in the lunar environment. Loading conditions on the voussoir dome were investigated to ensure that the structure could support itself. Also calculated was the potential of a voussoir dome structure from bricks fabricated though geothermic reactions.

The work of Faierson et al. [13] was one of the few research efforts to investigate the material properties of the created sintered material. They highlight that material strength is a function of the ratio of simulant to aluminum, as well as the grain size of the simulant used. However, there was little investigation into the differences in material strength as a function of the material composition. There was no study of the material's porosity. A main focus was to determine if the selected voussoir dome was suitable for manufacture from this sintered regolith and aluminum reaction. One feature of the voussoir dome is that it is compression stabilized. This structure is comprised of individual blocks, and for the dome to work, a variety of blocks and molds are needed, increasing the complexity of manufacture and assembly. Furthermore, an assembly

procedure for the structure would need to be developed for either autonomous or manned construction. In order to make this process completely ISRU based, it would be necessary to import equipment to refine aluminum and supply NiCr wire or develop a lunar resource-based alternative to complete the fabrication process.

Hobosyan and Marturosyan [14] investigated another type of thermitic reaction that produced structural material. JSC-1A lunar regolith simulant was mixed with aluminum and Teflon and tested in 0.133 Pa (10^{-3} Torr) vacuum conditions. The samples were prepared using a uniaxial press and measured at 13 mm in diameter and 3 mm in height. Material properties collected included Knoop Hardness, a microhardness test typically used for thin sheets or very brittle materials where only a small indentation may be made for testing purposes. A pyramidal diamond point is pressed into the polished surface of the test material with a known, often 100 g-force, load. Knoop Hardness measurements of 750 (100 gf) to 850 (1 kgff) were reported. Porosity was calculated for the end material at between 40% and 60%. Findings included a maximum combustion temperature of 1400 °C and a very rapid temperature rise of 500 K/s. A self-sustaining reaction could be achieved by combining 12% by weight concentration of aluminum with 1.5% of Teflon by weight. Higher Teflon concentrations lead to higher porosity, where inter-connected pore sizes varied in the range of 20–200 μm. The chemical reaction and thermal conditions of the reaction were the main focus of this research.

This work offers further insights about the possibilities of an additive-based sintered material, but did not fully investigate the final structural material properties. No compression testing was performed or other material properties investigated. Porosity was calculated but no correlation between porosity and material strength or other material properties were performed. No comparisons of hardness were made, however the reported Knoop Hardness is comparable to Quartz, 820, or Feldspar, 560. Notably, the combustion reaction took place under vacuum conditions, allowing for a more accurate lunar fabricated material sample. However, no investigation was done of the equipment required or for the operational difficulty of fabricating structural material on the lunar surface.

Balla et al. [15] demonstrated direct laser fabrication using JSC-1AC as a viable additive manufacturing method using Laser Engineering Net Shaping (LENS). Typically used in metal sintering, this process results in net-shaped parts ready for cleaning with minimal post-fabrication finishing. "Net-shaped" part is an industrial manufacturing term meaning that there is little need for extensive finishing work, such as machining or grinding. This system focuses a laser beam on lunar simulant with a spot size of 1.65 mm, causing its complete melting and then solidification. Particles must be screened to a range of 50–150 μm. Dense solid cylindrical parts, 8–10 mm in diameter and with a height of 25–30 mm, were produced using a 50 W laser, at a scan rate of 20 mm/s and a powder feed rate of 12.36 g/min. The powder feed rate is the rate at which the regolith is deposited onto the work plane. The work plane is also called the construction surface in other additive manufacturing processes. A laser energy density of 2.12 J/mm appeared to be ideal for generating the melt pool necessary for lunar regolith powder deposition without excessive liquid pool spreading or the cracking of solidified parts. While this testing was performed in ambient, non-vacuum conditions, the authors did suggest that parts made on the Moon should be stronger as the process performs better in a vacuum.

This work was a very detailed investigation of the parameters needed to produce a solid usable material from an additive manufacturing process. It offers insight into the energy requirements and the speed at which a LENS machine could produce useful material. While mentioned, this work did not include a thorough overview of what it would require to operate a system like this on the Moon. Regarding implementation using ISRU, the LENS system would need to be exported to the Moon for production. Material properties were not investigated, opting to leave this as future work. Since the simulant was completely melted, no porosity was computed.

A large-scale additives manufacturing system was investigated by Cesaretti et al. [16] to produce 1:1 scale structures using lunar regolith simulant. The goal was to design a preliminary lunar outpost structure, develop a lunar simulant and to demonstrate the construction process. Using a 3D-printing system called D-shape, samples and sizable structures were constructed with the machine's systems evaluated in both ambient and vacuum conditions of 1×10^6 mbar. A total of six liquid ink injections were tested with the nozzle buried in the simulant at vacuum conditions to determine if injections below a simulant layer could prevent the fluid from vaporizing. For terrestrial printing fabrication the printer does not bury the nozzle in the working material.

Rather than procuring a large quantity of JSC-1A or CAS-1, simulant DNA-1, based on natural volcanic material found close to the Bolsena Lake in Italy, was created. DNA-1 was also compared to JSC-1A and lunar soil sample 14,163. Of note, DNA-1 contains a larger mass percentage of MgO than JSC-1A but less than the lunar soil sample 14,163, and a smaller mass percentage of Fe_2O_3 as compared to JSC-1A. A large amount of MgO is a required reactant for the D-shape printing process.

The D-shape printer had a square work area of 6 m by 6 m and the printer head was 6 m long and used 300 nozzles in a line spaced 20 mm apart. Binding liquid is dropped onto the surface after a fresh layer of working material has been moved atop the work plane. While this is suitable for terrestrial construction, the authors state that this system would have to be reengineered before it would be functional on the Moon. Measurements of some mechanical material properties were performed for the fabricated samples, most notably: compressive strength of 20.35 MPa (2951 psi), total open porosity 13%, density 1855.33 kg/m^3, and Young's modulus 2350 MPa (340.8 ksi). In addition to structural use, an alternative use for solar radiation or micrometeoroid protection was also suggested.

The successful demonstration of constructing a large-scale structure using an additive manufacturing process from lunar simulant is a notable milestone for lunar structures technology. The system was proven to work in ambient conditions; the binding agent could work in a vacuum with some process modification. The details of the vacuum testing would need to be elaborated upon and structure construction tested in a larger format. The vacuum testing served the purpose of validating that the binding agent could bind the simulant in a vacuum environment. Some details of this process need to be elaborated for proper comparison with ISRU based manufacturing systems, such as how much binding liquid is required to produce the structures presented in their work. We will further discuss material property values presented in this work in subsequent sections.

Cardiff and Hall [17] sintered JSC-1A/JSC-1AF lunar simulants using concentrated solar energy through a Fresnel lens. Based on a rolling chassis, the Fresnel lens achieved a maximum sintering rate of 13 cm^2/min, sintered to about 0.5 cm deep. This test was also performed in a high vacuum on Earth, utilizing terrestrial solar rays; lunar solar rays would be more powerful as they do not have atmospheric obstructions. The maximum depth achieved was about 2.5 cm using this system. The Fresnel lens system, as demonstrated, served to prove the concept of a dust mitigation system. Extrapolating on the sintering rate measured, a construction rate was calculated. Within approximately a 55-day period, 100 m^2 of lunar regolith could be converted into a landing pad. This system could be almost entirely constructed using ISRU, making this process highly efficient. Sintering benefits from a vacuum environment, solar energy is readily available and raw lunar regolith is of course plentiful. With some additional complexity, similar to a 3D printing machine, it is possible to imagine a system utilizing a 3D printing base and a Fresnel lens to produce complex sintered lunar regolith structural components.

Gualtieri and Bandyopadhyay [18] investigated sintered lunar regolith material properties concurrently with this research project. The samples used in their testing were the same type of samples that they provided to us for testing. The simulant they used was a mix of JSC-1, JSC-1AF, and JSC-1AC lunar mare regolith simulant. The simulant

powder was sieved and separated into different sizes of greater than and less than 212 μm particles. Using 12.7 mm and 7 mm diameter cylindrical dies, samples with a height to diameter ratio of between 2:1 and 1.5:1 were pressed up to approximately 145 MPa. After pressing, the samples were fired for 20 min at 1200 °C. The phases of the sintered samples were analyzed and compared to the phases in the original powder using X-ray diffraction. The microstructure was observed using a field emission scanning electron microscope. The density of the samples was calculated using Archimedes' method. Compression tests were performed on a universal testing machine with a constant stroke rate of 0.5 mm per min until fracture. Hardness tests were conducted using a Vickers micro-hardness tester at a load of 100 g with a dwell time of 15 s. Melting was not noticed, however, liquid phase sintering was observed. They hypothesized the variation of porosity is a result of the different green densities of the starting state of the samples. Green density is defined as the weight per unit volume of an unsintered compact. Gualtieri and Bandyopadhyay [18] also noted that it is common for ceramic bodies being pressed by a die to have higher porosity near the edges of the sample due to frictional forces which cause a porosity gradient from the surface to the inside.

The material properties they reported were averaged from at least ten tests. The average hardness was 1030.2 $HV_{0.1}$ ± 69.73 $HV_{0.1}$. The hardness results were quite high and compared to commercial grade zirconia. Their 99.0 ± 0.5% dense samples had a failure stress that averaged 232 MPa and an average modulus of elasticity of 10.9 GPa. The 92 ± 2% dense samples exhibited a failure stress of 103.2 MPa and an average modulus of elasticity of 5.98 GPa. The Ryshkewitch equation was also used to calculate zero porosity compressive strength value of approximately 140.7 MPa. Also suggested was the feasibility of pressing a sample, then firing it in an oven.

Happel et al. [19] arrived at the conclusion that cast basalt would be the most suitable material to construct a lunar base from native lunar materials. The selection of cast basalt was based on internal pressurization, radiation shielding, construction ease, and manufacturing process size constraints of components. An ideal lunar construction material is one that is readily available in large quantities on the lunar surface and requires minimal processing. Minimal material preparation is needed except for filtering of lunar rocks greater than 18 cm. Once placed in a furnace, the basalt could be melted and poured into molds to cool. However, aside from its workability, a primary disadvantage of cast basalt is that it is brittle. Corrective measures of reinforcing cast basalt were discussed. Calculations based on an assumption that cast basalt has a mass density of 3 g/cm^3 showed an ultimate compressive strength of 538 MPa (78,000 psi) and a modulus of elasticity 100 GPa (14×10^6 psi). A process of manufacturing a cylindrical habitat from cast basalt was proposed.

The use of cast basalt as a lunar construction material is very appealing. The assumed compressive strength values are extremely high and require further verification. Testing in a reduced gravity environment should be conducted to verify the accuracy of terrestrial values of cast basalt. Gravity could play a role in crystallization during cooling and solidification of a cast material. Structurally, cast basalt is very strong, so strong that it might be over engineered and even wasteful regarding the energy used to melt and pour the basalt. An alternative to melting the lunar regolith is sintering, which would require less energy. Even if sintering produced a weaker material, it should be sufficient from a structural point of view in the reduced-gravity lunar environment.

McLemore et al. [20] performed the earliest test of sintering lunar regolith simulant by rapid prototyping methods at the NASA Marshal Space Flight Center using an electron beam melting (EBM) process. This technology uses an electron beam in a vacuum to melt metal powders layer-by-layer. The focus of the work was to produce metallic parts in situ. Testing was performed with granular titanium to produce mechanical components successfully before proceeding to lunar simulant. Only qualitative testing was performed using the Geological Survey Lunar Highland Type Medium NU-LHT-1M lunar regolith simulant. Light sintering of the simulant was observed, but no mechanical evaluation of the produced sintered material was reported. Nondestructive evaluation (NDE) techniques were also cited as a requirement for any part produced in situ for post-production quality inspection and certification. Laser ultrasonics was one potential NDE method proposed for post manufacturing certification. A combination of additive and more traditional subtractive manufacturing techniques will be needed for fabricating parts on the Moon.

Ray et al. [21] Characterized JSC-1A using DTA, TGA, XRD, chemical analysis and Mössbauer spectroscopy. Their work quantified the rate of cooling for JSC-1A melt and determined it to be 52 ± 1 °C/min.

1.3.4. What could Be constructed from ISRU lunar materials

Ruess et al. [22] performed a thorough structural engineering design and analysis of a lunar structure. Potential lunar materials were compiled from previous research works and included metals, fabrics, composites, indigenous materials and concretes. Material selection was cited as being a subjective process and mentions that cast regolith appears to have the best combination of material and manufacturing properties for ISRU materials. Types of lunar assembled structures were evaluated and compared. A design was settled upon with loading requirements established and finally, a detailed structural analysis was completed for a modular second generation lunar structure.

Wilson and Wilson [23] proposed sintering regolith or using epoxy paving as methods of mitigating lunar dust in the context of protecting a proposed lunar based, 20-m liquid mirror telescope. Coating the lunar regolith surface in either the epoxy or sintering the lunar regolith surface directly was discussed as a dust mitigation method. Long-term issues include, surface erosion, wear resistance, maintenance and damage repair from cosmic rays and/or micrometeoroid impacts.

Hintze et al. [24] investigated the potential of using two methods for dust mitigation on the lunar surface. The first was by sintering the regolith simulant into a solid with a solar concentrator. The second was by using heat or UV cured polymers to stabilize the surface. The solar concentrator was comprised of a Fresnel lens with a 1 m^2 collection area mounted on a moveable frame. Temperatures achieved by concentrating the Sun's rays through the Fresnel lens system were measured at 1350 °C, which was more than sufficient to melt the JSC-1A. The maximum depth to which the lunar simulant solidified was about 6 mm through a combination of melting and sintering. A decreasing of the JSC-1A density was observed during melting and the melted area appeared to contract, resulting in a weak bond between successive passes of the solar concentrator. A difficulty was that a single lens solar concentrator must move to follow the Sun if it is to maintain a focal point on a select spot resulting in difficulties to heat the lunar simulant to great depths or wide areas. A solution was to decouple the solar collector from the applicator. Greater depth could be achieved by sintering the surface layer by layer, or continuously adding regolith on top of the heated area. They also suggested regulating the sintering rate as a function of the measured sintered surface temperature. To provide an idea of the speed at which this process could construct, the time needed to sinter a specific size launch pad was calculated.

Load bearing tests were also conducted using the sintered and the polymer-cured materials. Strengths ranged from 130 psi for 2.5 mm thick samples, 290 psi for 4.2 mm samples to 310 psi for 6.0 mm samples. The polymer mixtures were able to reach strengths from 20 psi to 80 psi. Abrasion resistance tests were also performed to investigate the potential of a rocket launching or landing on the dust mitigated surfaces.

The most important outcome of this experimental research was the creation of a solid surface on top of the lunar simulant, proving that this dust mitigation method may be an option. More conceptually and not discussed in their research, these manufacturing methods have potential to manufacture structural components as well. On the Moon, it should be expected that sintering is more effective due to the vacuum conditions. This work was performed in the Earth atmosphere, and from the Earth's solar concentration of the sun. The more intense solar energy of the lunar

surface should also provide higher temperatures, allowing for increased rates of sintering if the temperature was properly regulated to avoid melting the lunar regolith. Sintered surfaces would be preferable to melted surfaces as melting caused contracting and cracking in the formed material. The number of load bearing tests were not mentioned, but assumed to be small due to the laborious nature of manufacturing the sintered components. For more accurate load bearing values, more specimens should be tested. The measurements from the load bearing tests should not be considered a maximum material strength value of the sintered material. Additional tests should be performed without the lunar simulant as a backing to understand the compressive strength of the material. Other mechanical material properties were not evaluated in this research. Use of UV based polymers adds complexity and a consumable non-in-situ resource, making UV polymers a less favorable option. Long-term thermal analysis of such a large solid structure was also not considered in the work. Presumably, a large solid sintered ceramic would undergo the thermal gradients of the standard lunar cycle and suffer from thermal fatigue.

1.4. A brief summary on sintering

To understand the importance of porosity in the sintering process, an understanding of how sintering works is important. We follow *Sintering Theory and Practice* by German [25] for this understanding. Sintering is a thermal treatment for bonding particles into a coherent, predominantly solid structure via mass transport events that often occur at the atomic scale. The bonding from sintering leads to improved strength and lowers system energy. This is not to be confused with melting which results in a phase transition of the material from a solid to a liquid. For a lunar application where resources would be limited, sintering would be more efficient at producing solid material than melting, require less energy since sintering occurs at about 50–70% of the melting temperature, depending on the material.

1.4.1. Gravitational affects on sintering

The traditional sintering process occurs in Earth's gravity. Sintering in the Moon's reduced gravity can be expected to be different quantitatively, but similar qualitatively. Microgravity experiments provide a hint as to these differences.

Upadhyaya and German [26] investigated data on liquid phase sintering (LPS) collected onboard the space shuttle Columbia during STS-65, STS-83 and STS-94 to study gravitational effects on tungsten heavy alloys. Tungsten contents range from 35 to 93% by weight with the matrix phase consisting of nickel and iron in a 7:3 ratio respectively. Tests were conducted in microgravity and terrestrial gravity. Tungsten heavy alloys are particularly sensitive to gravitation effects since the liquid-solid density difference is large. Using tungsten heavy alloys, samples were isostatically cold pressed, pre-sintered and then dry machined to cylindrical pellets.

In the terrestrial gravity field, gravity-induced grain settling results in solid-solid contacts that lead to coalesced grains. One recognizable problem in compacts sintered terrestrially is that gravity-induced solid-liquid separation and compact slumping when excess liquid is present. In LPS, an excess of liquid causes shape loss, consequently only alloys with small quantities of liquid, less than 20% by volume, are fabricated on Earth. The factors causing distortion in LPS are not understood.

Ideally, when a high liquid content alloy is sintered in microgravity it will try to minimize its energy by attaining a spherical shape. During microgravity sintering, the cylindrical pre-sintered sample underwent reshaping and completely spheroidized. Spheroidizing is a type of heat treatment for heavy metal-based alloys typically used to increase ductility. It is conducted at elevated temperatures just below the melting point of the material and is followed by a slow cooling. In terrestrial gravity the sintering alloy slumps and attains a ‘bullet’ shape. Pore evolution proved stable in microgravity. When sintered on Earth, pores are located on the top of the sample, whereas in microgravity pores are localized at the center of the sample. Conditions during sintering that cause the loss in structural rigidity prevail in microgravity. Microgravity sintered tungsten alloys disprove the premise that absence of gravity will lead to homogeneous microstructure during sintering. When low solid content alloys are sintered in microgravity they exhibit microstructural gradients from the periphery to the center of the compact. Under terrestrial conditions, distortion is accompanied by solid-liquid segregation, whereas in microgravity, the compacts tend to spheroidize. This implies that the conditions that cause the loss of structural rigidity prevail even in a microgravity environment.

German [27] commented on distortion due to the effects of gravity on LPS. Seventy-seven powder compacts have been processed in microgravity conditions with the following general observations: terrestrial gravity compacts always densify prior to distorting; gravity induces grain settling, with top-bottom grain size, solid volume fraction and contiguity gradients; grain settling does not occur in microgravity, rather surface to core gradients arise; pore elimination (densification) is essentially impossible in microgravity; pore coarsening and coalescence produce large pores in microgravity; green body homogeneity is a dominant factor with respect to distortion on Earth; grain settling induces structural rigidity that helps minimize distortion on Earth, without grain settling microgravity sintering results in more distortion. The overall observation was that samples are more porous and more distorted when compared to Earth-based sintering. Microgravity results in a lower strength compact since there is no grain compression to form a solid skeleton. As pores cluster and coalesce, they become closed but not eliminated. As a consequence, microgravity compacts are weaker with more distortion and less densification.

Park et al. [28] analyzed data collected aboard the space shuttle Columbia during STS-65, STS-83 and STS-94 to study the gravitational effects on LPS. Densification and distortion of liquid phase sintered tungsten heavy alloys were reviewed. Tungsten contents range from 35 to 93% by weight with the matrix phase consisting of nickel and iron in a 7:3 ratio, respectively. Tests were conducted in microgravity and terrestrial gravity. Lunar and Martian gravity conditions were investigated by means of interpolation between these two data points. The simulation results showed that gravitational forces are dominant in stronger gravity fields and surface tension effects are dominant in weaker gravity fields. The material composition also plays a role in distortion. Notably, with an increasing amount of tungsten (solid), the shape distortion was reduced in both microgravity and at terrestrial gravity but with less effect under microgravity.

Table 1 shows the general differences between terrestrial and microgravity sintering. Sintering tests have been conducted in terrestrial gravity and microgravity environments in an attempt to study gravitational affects. To date, only interpolation between these two data points has been used to predict the effects of sintering in the lunar gravity. The exact effects of lunar gravity sintering are not well understood and would require further testing to have quantifiable values. ISRU based sintering on the Moon would rely on ceramic sintering not metallic sintering, as has been studied in microgravity. It would be expected that sintering on the Moon would produce conditions between terrestrial gravity and microgravity.

1.4.2. Gravitational affects on this research

Our samples for this research have, of course, been fabricated in the

Table 1
Summary of sintering differences [27].

Attribute	Terrestrial Gravity	Microgravity
Densification	Yes	No
Distortion	Some	Considerable
Porosity	Little	Considerable
Pore Size	Small	Large
Buoyancy	Yes	No
Contiguity	High	Low

terrestrial gravity field and may have stronger characteristics than if the samples were to be sintered under lunar gravity. To what degree terrestrial sintering may have made these samples stronger than their lunar analogue is difficult to predict. This serves to highlight that further work is required to understand manufacturing by sintering within lunar gravity. LPS occurs as a result of sintering lunar regolith. However, it is currently unclear how the potential effects of centralized pore concentration and increased shape distortion on components sintered on the lunar surface could affect material properties and material strength. However, once these effects are better understood, it is surely possible to correct for pore concentration and distortion effects in order to regain or enhance lunar sintered component strength.

Whereas the microgravity research of Upadhyaya and German [26] was conducted using a very dense metal, the JSC-1A analyzed in our research is neither metal rich nor comparatively high density. Tungsten's density is about 19 g/cm^3 whereas solid basalt, which can be comparable to JSC-1A lunar simulant, has a density of about 3 g/cm^3. Samples fabricated on the Moon instead of terrestrially would result in shape and structural differences. There could be more shape distortion and different pore migration. Where the samples tested were all deemed cylindrical enough to test, it is possible that samples manufactured in a lunar gravity environment could have a pore structure localized at the center of the sample, and potentially more shape distortion. It appears that much of the microgravity sintering research to date was based on metallic sintering due to the large density gradients achievable. So long as metallic sintering is comparable to ceramic sintering, the metallic sintering microgravity-based research should scale appropriately for a lunar regolith analogue.

After reviewing the literature on the process of sintering and gravitational effects, we conclude that sintering can be a favorable manufacturing method for forming solid material in the lunar environment. We do not do an energy analysis of this process, but this is an important study required to demonstrate the economic viability of such a process. While we expect that this process would not be economically viable during the initial stages of lunar settlement, we also expect that the growing lunar infrastructure will improve economic viability.

2. Simulants

Across the entire American Apollo and Soviet lunar sample return missions, 382 kg and 300 g, respectively, of lunar material have been brought to Earth. Of this mass, significantly less was lunar regolith, making lunar regolith a highly valued material. Due to the scarce supply of lunar regolith, many lunar regolith simulants have been created over the years for various research projects. A list of known lunar regolith simulants was originally compiled by NASA's Marshal Space Flight Center [29] and expanded upon for this research is provided in Table 2.

A simulant must replicate the lunar surface as well as possible. Lunar regolith is substantially unlike any terrestrial material because of the lack of weathering effects from wind, water and erosion on the Moon. Depending on the application, a simulant is developed to mimic certain traits such as chemical composition, geotechnical properties or bulk properties. Simulants are typically developed based on data from the returned Apollo samples. Depending on the specific purposes of a test, one selects a particular simulant from the many specialized simulants.

With so many simulants available from so many different countries and of various base materials, it can be difficult to select the most appropriate simulant for an individual research problem. Another difficulty is accurately comparing results with similar research in the literature when different lunar simulants are used. To assist in evaluating lunar simulants, Rickman et al. [30] used a set of four standards: particle size-distributions, particle-shape distributions, density of the bulk material, and the relative abundance of minerals rocks and glass. In its ideal form, a researcher should be able to determine which of the four criteria are of most importance to their work, and then review the literature for the simulant that matches their need.

Table 2
Listing of known lunar simulants.

Simulant Name	Information	Type
ALS	Arizona Lunar Simulant	Low-Ti mare (geotechnical)
BP-1	KSC/Arizona Black point quarry waste (basalt); used for large excavation exercises with BLADE. Rahmatian and Metzger. (2010)	Low-Ti mare (geotechnical)
CSM-CL	Colorado School of Mines - Colorado Lava. Unpublished	Geotechnical
DNA-1	Cesaretti et al. (2013)	Low-Ti mare (general use), similar to JSC-1, higher MgO content
GCA-1	Goddard Space Center. Taylor et al. (2008)	Low-Ti mare (geotechnical)
GRC-1 & GRC-3	Glenn Research Center (Sandy, clay mixture used in SLOPE Facility for mobility/ excavation. Oravec et al. (2010)	Geotechnical: Standard vehicle mobility Lunar simulant
GSC-1	Goddard 'simulant"; material from local site that is being used for drilling testing	–
JSC-1	Johnson Space Center. McKay et al. (1994)	Low-Ti mare (general use)
JSC-1A, JSC-1AF, JSC-1C	Orbitec created under a NASA contract	Low-Ti mare (general use). Produced from the same source material as JSC-1
MKS-1	Carpenter. (2005)	Low-Ti mare (intended use unknown)
MLS-1	Minnesota Lunar Simulant Weiblen et al. (1990)	High-Ilimenite mare (general use)
MLS-1P	Weilblen et al. (1990)	High —Ti mare (experimental, not produced in bulk although small quantities were distributed)
MLS-2	Tucker et al. (1992)	Highlands (general use)
NU-LHT-1M, NU-LHT-2M, NU-LHT-1D, NU-LHT-2C	NASA/USGS Highland type simulant (chemical/ Mineralogical & physical properties) Stoeser et al. (2009)	Highlands (general use)
CAS-1	China (Chinese Academy of Sciences) a basic simulant made to represent Apollo 14	Low-Ti mare (general use)
CLRS-1	Chinese Lunar Regolith Simulant. Chinese Academy of Sciences (2009)	Low-Ti mare (general use?)
CLRS-2	Chinese Academy of Sciences (2009)	Low-Ti mare (general use?)
CUG-1	China. He et al. (2010)	Low-Ti mare (geotechnical)
NAO-1	NAO-1, National Astronomical Observatories, Chinese Academy of Sciences. Li et al. (2009)	Highlands (general use)
TJ-1, TJ-2	China (Torgji University); a basaltic ash feedstock with olivine and glass. Jiang et al. (2011)	Low-Ti mare (geotechnical)
CHENOBI	Canada (physical a& chemical properties simulant)	Highlands (geotechnical)
OB-1	Canada, Olivine-Bytownite. Battler and Spray (2009)	Highlands (general use geotechnical)
FJS-1 (type 1), FJS-1 (type 2), FJS-1 (type 3),	Fuji Japanese Simulant. Kanamori et al. (1998)	Low-Ti Mare, Low-Ti Mare, High-Ti Mare, (general use)
Oshima base simulant	Syeyoshi et al. (2008)	High-Ti mare (general use)
Kohyama base simulant	Syeyoshi et al. (2008)	Intermediate between highlands and mare (general use)
KOHLS-1	Korea. Koh Lunar simulant. Jiang et al. (2010)	Low-Ti mare (geotechnical)

One concern with lunar simulants, as indicated by Rickman et al. [30], is the sampling bias of the lunar samples. When considering average regolith properties, we are considering a mathematical construct that does not exist. Furthermore, the rocks and regolith returned from the Moon were handpicked by astronauts who typically favored their respective geology training. Samples were deliberately selected, not randomly selected, and thus are not statistically representative of the general population.

Another limitation identified was the lack of data available for very small grain size regolith of less than 5 μm. Simulants may have accurate averages of grain size, however, when matching grain size distribution of actual samples to simulant samples, this distribution does not always follow the same formula.

For our research, the distribution of particle size is the most important factor for the sintering investigation, especially since it factors into the green density of the compact which impacts porosity. Since our goal is the use of unrefined regolith and the effects of porosity, particle-shape distribution and bulk material density are considered secondary in our simulant selection criteria, even though they may be important to other considerations.

Material composition is of considerable importance as different ratios and types of materials can lead to different melting temperatures, which could impact the sintering process. Also impacted are the types of sintering possible, as mentioned previously, inclusions of nanophase Fe^0 allowed microwave sintering to take place. For this research microwave sintering was not to be investigated, making this addition not necessary. Rickman et al. [30] point out that the regolith is very different between the mare and the highland areas, and even there it is not uniform.

In the United States, the JSC-1 has become the industry standard. JSC-1A is a family of low-Ti mare lunar regolith simulants typical in the lunar mare regions. It was designed to be as similar as possible to its predecessor JSC-1 and was produced from the same source material. Ultimately the driving factor for lunar simulant selection became a function of availability and economics, and we pursued our studies using JSC-1A.

2.1. Samples from simulant

JSC-1A simulant was sent to Bandyopadhyay and Gualtieri, of Washington State University, Pullman, pressed and oven-fired to generate specimens. Two sample sets of eight each were produced to evaluate the effect of porosity on the material properties. Details of the sintering process can be found in Gualtieri and Bandyopadhyay [18], with a summary below.

The powder was first sieved to separate out any grains that were larger than 212 μm. Six grams of the powder was then poured into a 12 mm wide cylinder mold. Next, the powder was pressed at 4 MPa for 1 min; producing a sample with a 2:1 height to width ratio. The samples were then sintered using a Zircar Hot Spot 110 furnace at 1120 °C for 15 min. Finally, the sample was inspected to ensure that the cylindrical shape was retained and the cylinder ends remained flat.

Two sintered batches of samples were produced. The fine powder that made it through the No. 70 sift with particles <212 μm, later became the low porosity sample set with a calculated average porosity of 1.44 ± 1.91% (n = 7). The remaining powder comprised of particles >212 μm was sintered into the 11.78% porosity sample set with a calculated average porosity of 11.78 ± 3.30%, (n = 9). Where s is the standard deviation and n is the sample size.

2.2. Physical attributes of the samples

Physical dimension statistics were measured and calculated for all of the samples evaluated. As shown in Table 3, the average sample from the 1.44% porosity group weighed 5.326 g, had a height of 19.104 mm and a diameter of 11.696 mm. From Table 4, the average sample from the 11.78% porosity group weighed 4.941 g, had a height of 18.857 mm and a diameter of 12.242 mm. Visual inspection was performed to ensure all samples were similar in concentricity of shape. All were, with the exception of sample number 8, which had a slight, cylindrical toroidal curve, but retained parallel faces at each end. Whereas all samples had a dull reddish grey color, the most noticeable visual differences were in the surface roughness. Attributed to the initial powder grain size, the 1.44% porosity material was much finer than the coarse grains of the 11.78% porosity samples.

A photograph of two representative samples can be seen in Fig. 1. The 11.78% porosity samples had noticeable voids on the surface and even fail to form a complete circle at the top of the cylinder, highlighted by a red circle. This inability of the samples to have a completely full faced profile is a potential reason for the several initial failures during testing.

3. Experimental apparatus and test procedures

Details of the compression testing process can be found in Indyk [31] with a summary below.

Compression testing was performed using an Instron 4500 Series Universal Test System running Series IX version 8.04.00 software. Testing parameters included the crosshead speed of 1.000 mm/min and break detection set to 5 kN. Data was recorded at 10 points per second measured load in kN and displacement in mm. The sample was placed between the compression plates of the universal test machine, and then preloaded to about 300 N. Additionally, video of each test was recorded and ambient room temperature and pressure conditions were observed for the duration of the testing.

4. Data analysis

4.1. Load vs. deflection relations

The most fundamental data recorded during compression testing of the axially loaded specimens were deflection and load. A standard nomenclature for this test series is sought to portray important points during the specimen loading and is presented here. The ultimate failure of the sample occurs at the ultimate load and ultimate deflection of the sample. If a sample ruptured prior to the ultimate failure, this is denoted as a local failure with the first in the series being the initial failure of the

Table 3
Sample physical dimension statistics for 1.44% porosity samples.

Sample Number	Mass (grams)	Average Height (mm)	Height STD (n = 3)	Average Diameter (mm)	Diameter STD (n = 5)	Average Density (g/cm^3)
1	5.430	19.585	0.0352	11.5718	0.0556	2.6363
2	5.346	19.0213	0.0019	11.6934	0.0537	2.617
3	5.391	19.359	0.0137	11.7222	0.0743	2.5805
4	5.650	20.538	0.0067	11.6624	0.0840	2.5755
5	5.488	19.424	0.0297	11.7292	0.0255	2.6151
6	4.724	16.9083	0.0597	11.6844	0.0380	2.6055
7	5.249	18.893	0.0373	11.8100	0.0731	2.5361
Mean	5.326	19.104	–	11.6962	–	2.5951
STD	0.271	1.023	–	0.067	–	0.0311
Variance	0.074	1.047	–	0.004	–	0.0010

Note: n = sample size, STD = standard deviation.

Table 4
Sample physical dimension statistics for 11.78% porosity samples.

Sample Number	Mass (grams)	Average Height (mm)	Height STD (n = 3)	Average Diameter (mm)	Diameter STD (n = 5)	Average Density (g/cm^3)
8	5.437	20.174	0.0153	12.0806	0.0927	2.3509
9	5.093	19.405	0.0594	12.1356	0.0487	2.2692
10	4.180	16.576	0.0430	12.5176	0.0484	2.0489
11	4.938	18.7863	0.0347	12.1434	0.0331	2.2694
12	5.106	19.8533	0.0399	12.1742	0.0999	2.2095
13	5.106	19.1503	0.0158	12.1378	0.0475	2.3043
14	5.048	18.7807	0.0194	12.1096	0.0293	2.3337
15	5.002	19.2723	0.0485	12.5304	0.0191	2.1049
16	4.555	17.717	0.0343	12.3468	0.0347	2.1475
Mean	4.941	18.8574	–	12.2418	–	2.2265
STD	0.344	1.0437	–	0.1667	–	0.0997
Variance	0.119	1.0892	–	0.0278	–	0.0099

Note: n = sample size, STD = standard deviation.

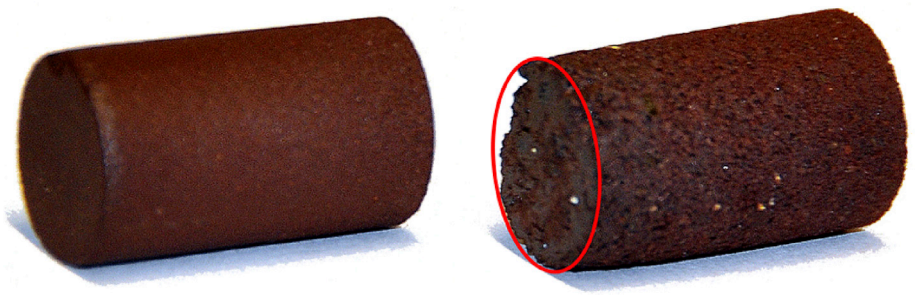

Fig. 1. Photograph of two representative samples, left is 1.44% and right is 11.78% porosity.

sample. Tests that demonstrated such initial and local failures were allowed to continue running until the ultimate failure occurred. Deflection values after the initial failure values lose significance since it is not clear if the deflection recorded is due to actual deflection or a failure of the sample.

Initial inspection of the data was performed to evaluate the quality of the data for each test. Multiple tests failed before reaching the maximum compressive load due to the brittle nature of the samples. Several samples exhibited an initial/premature failure, with a representative example clearly seen in Fig. 2. After the initial failure, the sample retained its integrity and was able to recover and withstand further loading until failing at the ultimate load. Of the seven tests for the 1.44% porosity set, three ran to completion without an initial failure. A single test, test number 5, had one initial failure and three tests, 2, 4 & 7, had multiple

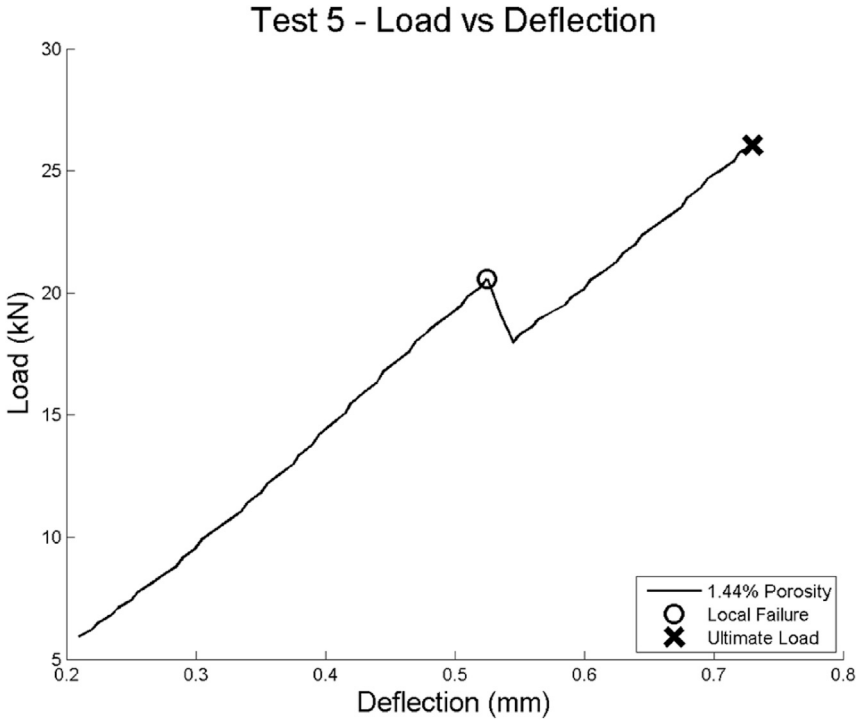

Fig. 2. Test 5, 1.44% porosity sample load vs. deflection with an initial failure at about 0.5 mm deflection.

local failures. Of the 11.78% porosity set, three ran to completion without an initial failure. Two had one initial failure, tests 11 & 14, and four tests, number 8, 10, 15 & 16, had multiple local failures.

Because these initial failures were so common in the testing, two calculations were carried forward in the data analysis, one for the initial failure values, and one at the ultimate failure values. The initial failures values were recorded in the hope of establishing a lower bound to the strength of the material. The ultimate failure values could be interpreted as the upper limit of the strength of the material if a more refined and consistent manufacturing process were to be implemented.

Investigating the effects of porosity on the loads and pressures achieved by each low and high porosity material is a key aspect of this research. The simplest approach to determine the effects of porosity is to average all the tests data regardless of the existence of premature failures. The average ultimate load for the 1.44% porosity data was 23.49 ± 2.41 kN, and 9.86 ± 3.93 kN for the 11.78% porosity data, where the format is mean value $\pm$ one standard deviation. The load achieved is unique to each sample and depended on the sample dimensions. This is a difference of about 13 kN between two porosity sets with only about 10% difference in porosity.

To take into consideration the dimensions of the samples, the average pressure is calculated for more accurate comparisons. The average maximum pressure for the 1.44% porosity data was 218.79 ± 23.54 MPa, and 84.56 ± 34.87 MPa for the 11.78% porosity data. Here, a difference of about 133 MPa is observed. The 1.44% porosity material withstood over two times the pressure than the 11.78% porosity material. A direct and simple conclusion can be made that porosity does have a significant effect on the loads and pressures the sintered material was able to resist. This was expected, but these results demonstrate how significant these differences can be.

For both data sets, three tests completed without initial failures of the sample. The average maximum load for these tests was 25.31 ± 0.79 kN and an average pressure 237.17 ± 10.05 MPa for the 1.44% porosity samples. The average load and pressure values for the 11.78% porosity data were respectively 11.68 ± 1.20 kN and 100.72 ± 10.51 MPa. These values represent the highest loading withstood by the samples. It is interesting again to note that the 1.44% porosity material withstood over twice the pressure than the 11.78% porosity material.

Inspecting the tests which an initial failure occurred, there does not seem to be a correlation pointing to a common load or pressure that provoked an initial failure. Searching for a cause for the premature failures, we considered the loading conditions. For both the low and high porosity data sets, five tests occurred with initial or premature failures of the sample. The load at initial failure average for the 1.44% porosity data set was 21.23 ± 4.08 kN and 8.32 ± 4.44 kN for the 11.78% porosity data set. Loading ranges including the first standard deviation for both the low and high porosity data do not overlap, suggesting that there is no statistically significant load for which the samples should be expected to prematurely fail.

There does not appear to be a relationship between local failures and maximum loads achieved on a per test basis for each porosity data set. For example, even though the 1.44% porosity specimen in test 5 experienced a premature failure at a high load, 20.57 kN, it was able to recover to a maximum load of 26.05 kN. This maximum load is comparable to that of test 1, 26.35 kN. Thus, sample 5 performed exceptionally well. Another 1.44% porosity specimen in test 2 reached about the same maximum load, 21.37 kN, with an initial failure load, 20.93 kN. An example from the 11.78% porosity sample set was the specimen of test 11, which was the best performing test in its set. Test 11 had an initial failure occur at 15.78 kN, which was less than 1 kN under its maximum load of 16.08 kN. Even after the failure, this specimen achieved the best performance of the 11.78% porosity material, about 3 kN better. Interestingly, *all tests in which initial failures occurred were still able to achieve the similar or greater maximum loads after the initial failure.* However, only in tests 5, 11 and 14 were the final load values able to match or exceed the final load values of their non-local failure counterparts. So more often than not, the tests without local failures were still able to achieve the highest loads. This is an important result.

Further investigating the load distribution after a sample experienced an initial failure, video from each test with an initial failure was analyzed. Not all premature failures were observed in video recordings, some reasons include that the angle of the camera was not facing where a failure of material occurred or the failure was so small it was not observable. Using test 5 as an example, shown in Fig. 3 is an images of the before and after the initial failure. The images used were enlarged and the contrast increased. After the initial failure, the upper right corner of the sample broke off. The angle of the failure is not perpendicular to the camera angle, so the projection of the missing corner is at an uncertain angle. But a cross sectional area change can be estimated assuming a perpendicular projection of the missing piece. The missing piece accounts for approximately 7% of the sample profile area, or more importantly approximately 6% of the total cylindrical volume of the sample. After the premature failure, the remaining material as to compensate and bear a higher concentration of load. Even with this dramatic example of material loss under load, this sample was able to withstand 50 MPa before reaching ultimate failure.

Because of this, it should be expected that samples with initial failures should generally not reach the same maximum loading as un-fractured samples. In general, this was the case. The average ultimate load for the three 1.44% porosity tests without initial failures was 25.31 ± 0.79 kN, and 11.67 ± 1.20 kN for the 11.78% porosity data set. Of the four low porosity tests with local failures only test 5 was able to exceed the final average load set by the three non-local failure 1.44% porosity tests. And for the five high porosity tests with initial failures, two tests, test 11 and 14, were able to exceed the final load average set by the three non-local failure 11.78% porosity tests. Of a total ten tests with local failures, only three tests were able to exceed the load average set by the tests without premature failures. Still, six samples of both porosity grades experienced nominal compression tests without failing prematurely. Since the tests with initial failures were able to approach but not meet the maximum loads as those samples without initial failure, the manufacturing process, not the material itself, requires further investigation in order to control the quality of the sample produced. Again, even with local failures, the 1.44% porosity material withstood over two times the pressure of the 11.78% porosity material. The results from the tests with local failures provide evidence that *even though the material itself may be brittle, it can hold high compressive loads even after fracture.*

Fig. 4 superposes all load-deflection tests, highlighting the two groups of sample data as well as the range of results. While there is variability, we can also see significant uniformity in the behavior. It becomes evident that the 1.44% porosity samples were able to sustain the highest loading conditions where the 11.78% porosity samples were able to sustain loads at about half the magnitude of the 1.44% porosity samples.

The initial failures reduced the ability of ten specimens to reach their full loading potential. The average pressure at initial failure achieved by all the 1.44% porosity samples was 197.80 ± 39.33 MPa, and 71.31 ± 38.89 MPa for the 11.78% porosity data with initial failures. Compared to the three tests in each data set without initial failures, a 17% and 30% average pressure difference for both the low and high porosity data set respectively could be expected if the samples had not experienced initial failures. The tests without initial failures are the most accurate values of pressure possible for the cumulative samples tested as the sample dimensions remained intact until ultimate failure. However, it is once again important to note that these pressure differences are expected to be reduced if the actual sample dimensional information was known after the initial failure.

On average, the 1.44% porosity material was able to sustain higher compression loads and deflection before failure than the 11.78% porosity material. Tables 5 and 6 summarizes loads and deflections for the data sets. The average deflection at the ultimate load for the 1.44% porosity data was 0.643 ± 0.034 mm, and 0.463 ± 0.041 mm for the 11.78% porosity data. The test that experienced the greatest deflection without

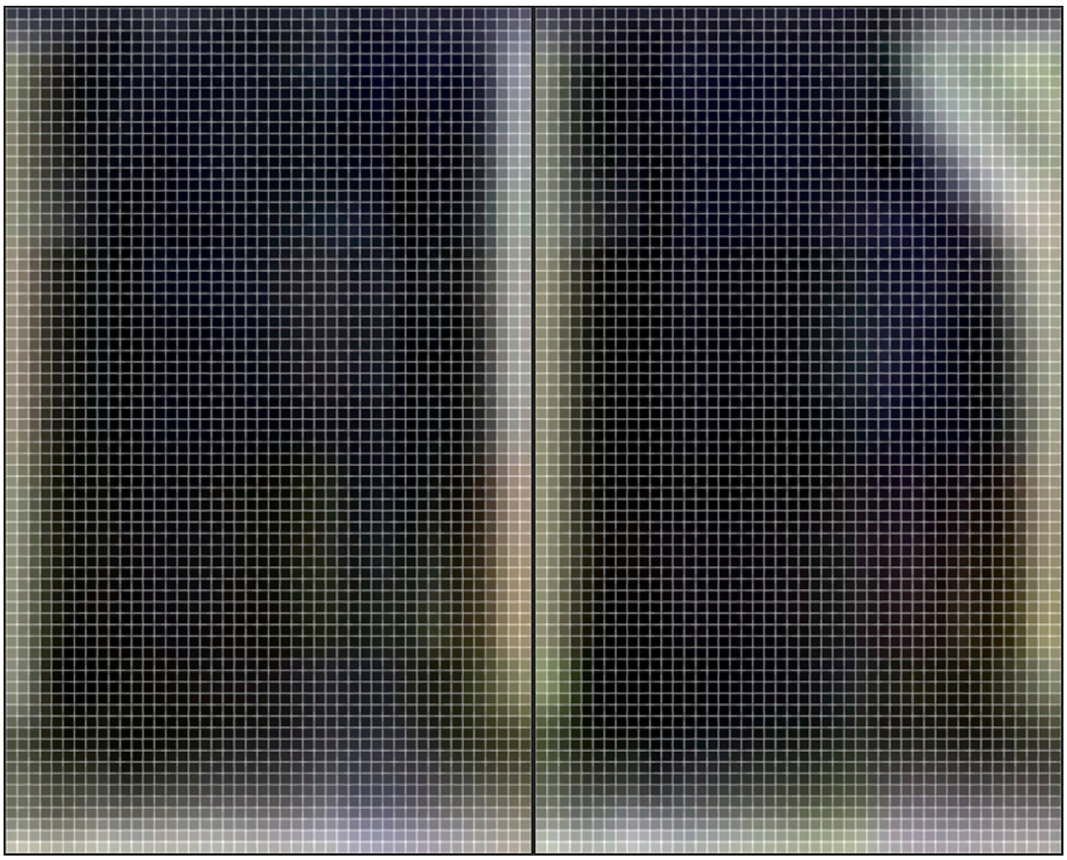

Fig. 3. Left: Sample 5 before initial failure. Right: Sample 5 after initial failure.

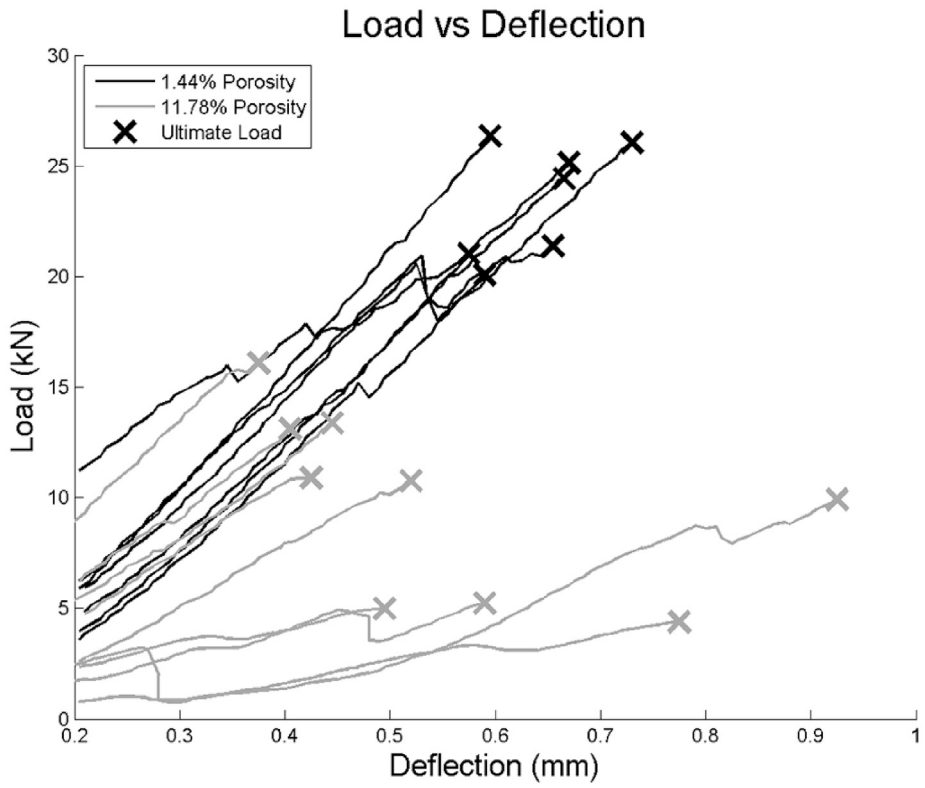

Fig. 4. Load vs. deflection of all tests.

Table 5
Loads and deflections for all 1.44% porosity tests.

Test Number	Load at Initial Failure (kN)	Ultimate Load (kN)	Ultimate Deflection (mm)
1	–	26.35	0.595
2[b]	20.93	21.37	0.655
3	–	24.43	0.665
4[b]	15.17	20.08	0.590
5[b]	20.57	26.05	0.730
6	–	25.15	0.670
7[b]	15.98	21.03	0.575
Mean	21.23	23.49	0.640[a]
STD	4.08	2.41	0.052[a]
Variance	16.67	5.80	0.003[a]

Note: STD = standard deviation.
[a] Only includes values from tests without initial failures.
[b] Tests with initial failures.

Table 6
Loads and deflections for all 11.78% porosity tests.

Test Number	Load at Initial Failure (kN)	Ultimate Load (kN)	Ultimate Deflection (mm)
8[b]	3.21	9.92	0.925
9	–	10.76	0.520
10[b]	3.32	4.38	0.775
11[b]	15.78	16.08	0.375
12	–	10.90	0.425
13	–	13.37	0.445
14[b]	8.91	13.12	0.405
15[b]	4.92	5.23	0.590
16[b]	3.74	4.99	0.495
Mean	8.32	9.86	0.551[a]
STD	4.44	3.93	0.175[a]
Variance	19.75	15.42	0.031[a]

Note: STD = standard deviation.
[a] Only includes values from tests without initial failures.
[b] Tests with initial failures.

encountering an initial failure was a 1.44% porosity sample, test 6, which deflected 0.670 mm. The largest deflection without an initial failure seen by an 11.78% porosity sample, test 9, which underwent 0.520 mm of deflection.

Computing stress, strain and elastic moduli is the next step in quantifying the material properties.

4.1.1. Stress, strain and modulus of elasticity

Of great importance to any material property investigation is an understanding of how well a material can handle and recover from stress and strain. The sintered lunar simulant specimens tested are more similar to ceramic materials, which typically fail due to small defects, than metals, which allow greater material deformation. No measurement device was available during testing to measure cross-sectional area change, but that was not a concern since the brittle nature of ceramics typically allow for minimal cross-sectional deformation before failure. Because of this, the difference in area is expected to be minimal, making engineering stress and engineering strain values relevant calculations.

Engineering stress $\sigma = F/A$, engineering strain $\varepsilon = \Delta L/L$, and the modulus of elasticity, E, were calculated based on a linear best fit for each data set. Using the averaged sample dimensions measured prior to testing, stress and strain for the duration of the test was calculated. A plot of the calculated stress strain relationship from test 1 and test 7 can be seen in Fig. 5. Sample 1 in test 1 exhibited textbook behavior for a ceramic type material enabling a clean modulus of elasticity calculation. Comparatively, tests with multiple local failures, as seen in test 7, made this calculation difficult.

The modulus of elasticity was calculated from the slope of the stress strain line for each test and averaged with the low or high porosity data set. Calculated from the start of the sample loading until the initial failure or ultimate failure of the sample, whichever was greater. Tests 7, 8, 10, 15 and 16 were omitted from this calculation due to poor stress-strain data, leaving six tests from the 1.44% porosity data set, and four tests from the 11.78% porosity data set. The 1.44% porosity modulus of elasticity was calculated to be 8358 ± 748 MPa, and the 11.78% porosity

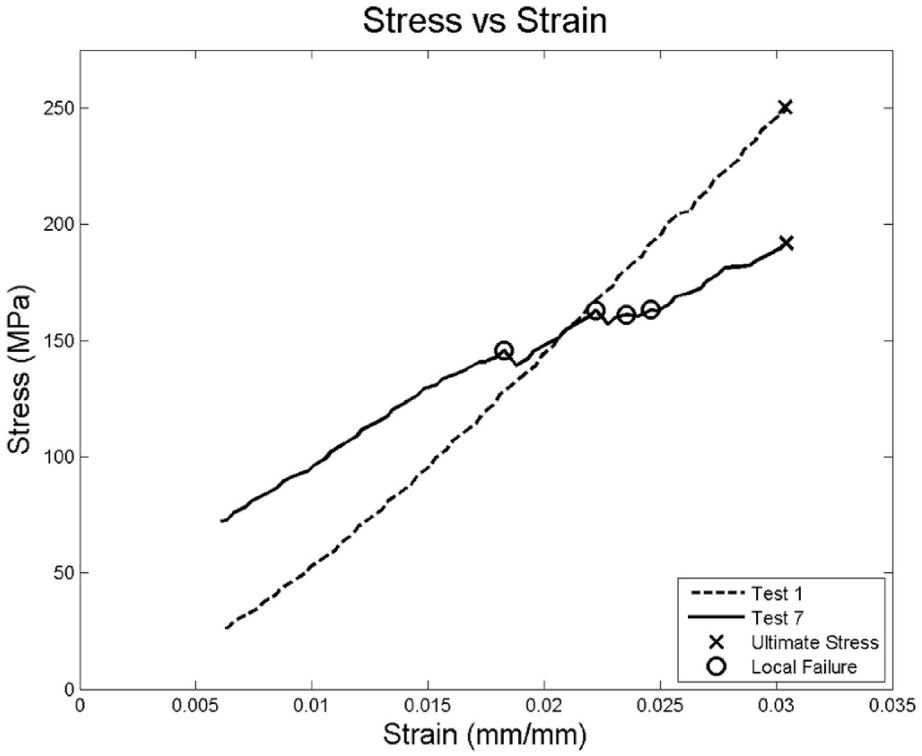

Fig. 5. Stress vs. strain for tests 1 & 7.

modulus of elasticity calculated to be 5475 ± 782 MPa. It is interesting to note that even though the mean values are quite different, the standard deviations are essentially identical, indicating a large coefficient of variation for the 11.78% porosity material.

4.1.2. Toughness

Material toughness describes a material's ability to absorb energy and resist fracture. Tough materials can absorb a considerable amount of energy before fracture while brittle materials absorb very little. Toughness is not a single property but rather a combination of strength and ductility. Materials with high yield strength and high ductility have high toughness. The toughness of a material can be determined by integrating the area under its stress-strain curve before fracture, with units of joules per meter cubed,

$$\int_0^{\epsilon_f} \sigma \, d\epsilon = \frac{energy}{volume} \tag{1}$$

where ε_f is the strain at failure. The stress strain data used was from the start of the ramping until the initial failure of the specimen. The early ramping region is expected to add a trivial amount of inaccuracy in the computed toughness values.

The calculated toughness values for each test are shown in Table 7. Averages with standard deviation were calculated for both data sets. The 1.44% porosity data calculated average was 3.2 ± 0.9 MJ/m^3, and the 11.78% porosity data average was 1.0 ± 0.3 MJ/m^3. These results are not surprising as the 1.44% porosity samples were able to withstand higher loads. What is interesting is that the 1.44% porosity samples demonstrated three times the toughness than the 11.78% porosity samples.

The samples without initial failure with the greatest deflection and load ratio respectively was test 6, this is the second highest toughness value after test 5, which did incur an initial failure. For the 11.78% porosity tests, sample 11 had the greatest calculated toughness. Test 13, which did not experience an initial failure, had the second highest toughness value of the 11.78% porosity sample. Sample 1 showed the greatest load bearing capacity but also the lowest deflection of the three 1.44% porosity, non-initial failure tests. Sample 5 resisted the second highest loading of all the samples tested, but achieved the highest calculated toughness. Material toughness is typically used to evaluate the ability of a material to withstand an impact. For lunar applications this could be a measure of resistance to meteoritic impacts.

4.1.3. Compressive strength

Compressive strength is defined as the strength at which the sample fails. The mode of failure may be either brittle or plastic and corresponds to a dramatic increase in strain given a small change in stress. Compressive strength is calculated by dividing the maximum load by the original cross-sectional area of a specimen in a compression test.

Table 7
Calculated toughness per test.

Test Number	Toughness (MJ/m^3)
1	3.2
2[a]	3.7
3	3.4
4[a]	2.2
5[a]	4.3
6	3.8
7[a]	3.7
8[a]	1.5
9	1.1
10[a]	0.7
11[a]	1.5
12	1.0
13	1.3
14[a]	1.2
15[a]	0.7
16[a]	0.6
Mean	3.2
STD	0.9

Note: STD = standard deviation.
[a] Tests with initial failures.

Table 8
Compressive strength at initial failure and maximum failure.

Porosity Data Set	Calculated Value	Initial Failure (MPa)	Ultimate Failure (MPa)
1.44% (n = 8)	Mean	197.8	218.8
	STD	39.3	23.5
	COV	0.20	0.11
	Variance	4508	2399
11.78% (n = 8)	Mean	71.3	84.6
	STD	38.9	34.9
	COV	0.55	0.41
	Variance	1512	1215
1.44% (n = 3)	Mean	-	237.2
	STD	-	10.1
	COV	-	0.04
	Variance	-	101
11.78% (n = 3)	Mean	-	100.7
	STD	-	10.5
	COV	-	0.1
	Variance	-	110

Note: n = sample size, STD = standard deviation, COV = coefficient of variation.

Results showing the sample values for compressive strength are seen in Table 8. Of interest are the compressive strength values of the 1.44% porosity samples. An average compressive strength for the 1.44% porosity data set was 218.8 MPa ($n = 7$). The samples without an initial failure averaged 237.2 MPa ($n = 3$). The highest compressive strength obtained was from sample 1, 250.6 MPa. The 11.78% porosity sample set proved to be more brittle and withstood a lower load than its sibling samples. However, the compressive strength values were still quite high. The average compressive strength of the entire 11.78% porosity data set was 84.6 MPa ($n = 9$). Samples without an initial failure in testing averaged 100.7 MPa ($n = 3$). The highest compressive strength obtained was from sample 11, 138.9 MPa, and the lowest was from sample 16, 41.7 MPa. *It is worth noting that the worst performing low porosity sample performed better than the average 11.78% porosity sample.*

The compressive strength values from the samples tested hold more significance when compared with the more common terrestrial structural materials as well as with better understood lunar concretes. Another appropriate comparison of sintered simulant is with basalt, as it is plentiful on the lunar mare regions. Basalt is also hailed as one of the strongest igneous rocks. Since the tested sintered lunar regolith simulant is also comprised mostly of basalt, the Dresser Basalt values can be seen as an appropriate upper strength limit for this sintered medium. Shown in Table 9 are the compressive strengths and selected tensile strengths for three grades of concrete, three common rocks and two proposed and tested lunar concretes.

Table 9
Comparative compressive and tensile strengths.

Material	Compressive Strength (MPa)	Tensile Strength (MPa)
Lunar sulfur concrete[a]	31	-
Lunar concrete[b]	74	8.3
Terrestrial concrete (residential)[c]	17	-
Terrestrial concrete (commercial)[c]	28	-
Terrestrial concrete (high strength)[c]	70	-
Kasota Sandstone[d]	102	6.3
Morton Granite Gneiss[d]	194	14.0
Dresser Basalt[d]	306	17.0

[a] Toutanji et al. [2].
[b] Lin [1].
[c] National [32].
[d] Bridgford and Eustes [33].

Comparisons between Tables 8 and 9 can be made. The strongest sample set, the low porosity samples, was able to reach 82% of the compressive strength of Dresser Basalt. We can also see from Table 9 that concrete has a high range of compressive strengths, from 17 MPa (2500 psi) for residential concrete, to 28 MPa (4000 psi) for commercial structures, and to higher compressive strengths up to and exceeding 70 MPa (10,000 psi). The compressive strength of the single best low porosity sample, sample 1, is very strong in comparison to concrete. Sample 1 was able to achieve almost 15 times the compressive strength of terrestrial residential concretes. Even the worst performing individual 11.78% porosity sample, sample 16, was able to achieve almost 2.5 times the compressive strength of terrestrial residential concretes. Comparing the single best low porosity sample, sample 1, to lunar concrete showed the low porosity material was almost 3.5 times stronger. These results suggest that sintering is a viable option for high strength applications for lunar construction.

While tensile testing was not conducted, it would not be expected that sintered lunar regolith would have a high tensile strength. Ceramics, concretes and rocks are typically brittle materials, and as seen in Table 9, all the tensile strength values are relatively low in comparison to their compressive strength. Hence, sintered lunar regolith would be suitable for compressive loads; however, tensile loading could be investigated further if it is anticipated that sintered regolith can be reinforced.

4.1.4. *Compressive strength as a function of porosity*

For sintered materials, porosity is a contributing factor to material strength. To determine an upper and lower bound of compressive strength related to porosity, averages and standard deviations of these two data sets were calculated and assuming a linear relation, linearly extrapolated. Initial and ultimate failures of the samples were evaluated to gage the upper and lower bounds of the material strength.

Assessing the maximum compressive strength obtainable related to porosity, Fig. 6 shows the compressive strength and porosity for ultimate compressive loading of the sample. Fig. 7 shows the compressive strength related to the compressive loading during the initial failures of samples. The 11.78% porosity data set produced a larger range of values, leading to a wider standard deviation bound. This can be attributed to the greater brittleness of this material. The 1.44% porosity data set had a higher compressive strength in both cases of initial and ultimate failure.

We cross-plot the two compressive-strength/porosity set of curves in Fig. 8, where we see an overlap. The trending of these equations is as expected, with the initial failures having lower mean values than the ultimate failures. Graphically it is observable how close are the initial and ultimate mean failures of the 11.78% porosity data sets. Also of interest is the close proximity of the first standard deviation upper bound. That both the initial and ultimate failure linear fits share a very similar slope attests to the consistency of upper range of the failure values. The lower bounds have more conflicting lines as expected since it is more common for a sample to fail prematurely as opposed to fail at an unusually high value.

As a way to compare these values with those of solid basalt, a major component of JSC-1A, we extrapolate to 0% porosity values. We find a compressive strength of about 237 ± 24 MPa for the ultimate failure data set, and an approximate value of 215 ± 42 MPa for the initial failure data set. The value measured by Bridgford and Eustes [33] for Dresser Basalt was 306 MPa. Our extrapolated 0% porosity value is, as expected, below the Dresser Basalt value.

Since porosity affects the structural quality of the sintered lunar simulant, there may be geographic limitations to where sintered lunar regolith could be manufactured on the Moon. The sample's achieved porosity is a function of the gain size of the lunar simulant used. This is an important observation as it is possible that different regions of the Moon contain higher concentrations of either fine or large grained regolith. Fortunately, data returned from the Apollo missions provide insights into regolith particle size, and analyses of Lunar Reconnaissance Orbiter (LRO) data have provided regolith depth estimates across the lunar surface.

Table 10 shows a breakdown of grain size fractions of two lunar samples. Sample 71061,1 was a typical Apollo 17 mare soil and sample 72441,7 a typical South Massif soil, both taken from the “light” mantle deposit. Using these as example regolith particle size distributions, it is

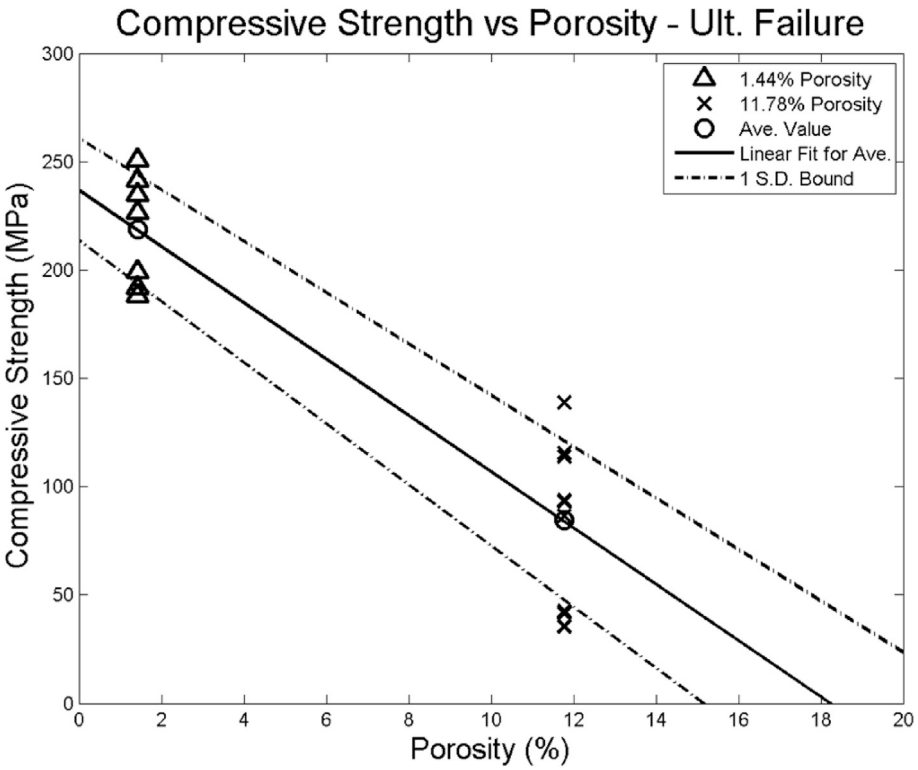

Fig. 6. Compressive strength vs. porosity at ultimate failure.

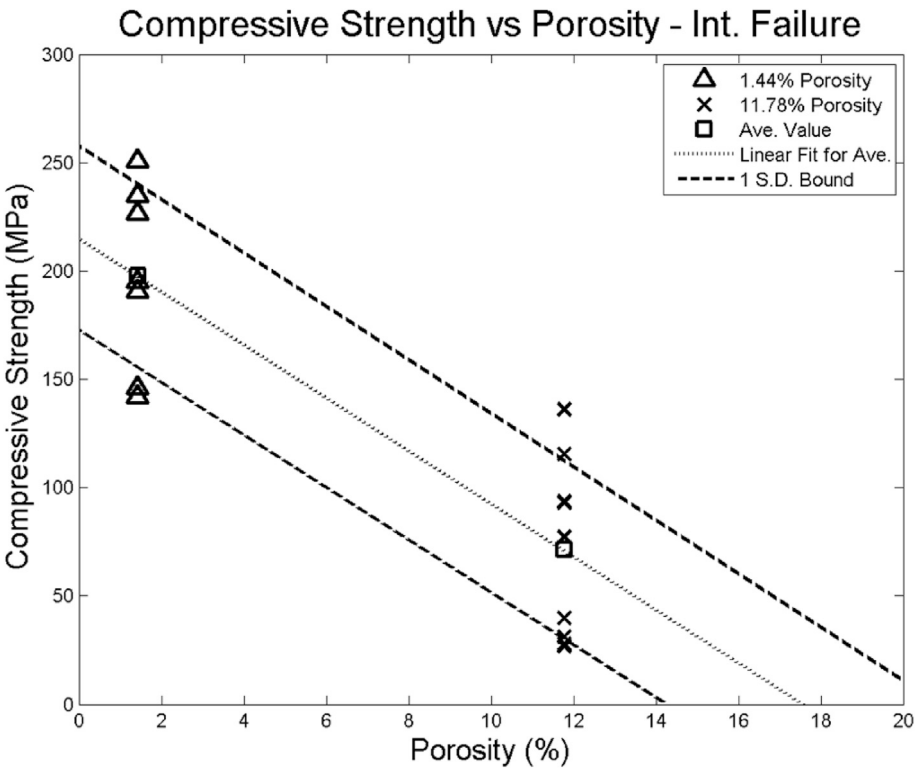

Fig. 7. Compressive strength vs. porosity at initial failure.

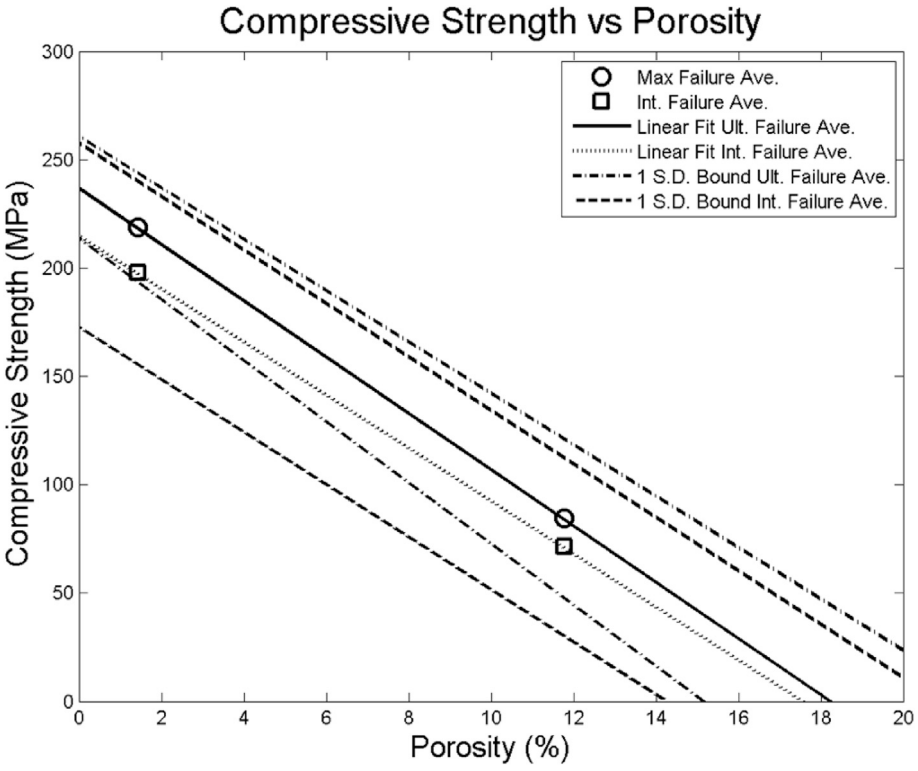

Fig. 8. Compressive strength vs. porosity.

possible to approximate the quantity of 1.44% and 11.78% porosity material that could be found at each sample site. Since a higher resolution breakdown of particle size is not available, for this analysis the weight percentage of 150–250 μm will be conceded to the greater than 212 μm category. For sample 71061,1 a total 50.24% of particles were below 150 μm in size, and 40.61% being greater than 150 μm. For sample

Table 10
Lunar sample particle size distribution sorted by weight percentage.

Sample	<20 μm	20–45 μm	45–75 μm	75–90 μm	90–150 μm	150–250 μm	250–500 μm	0.5–1 mm	1–2 mm	2–4 mm	4–10 mm	Sum
71061,1	17.98	12.21	8.39	3.00	8.66	7.04	7.08	3.44	6.15	6.74	10.16	87.85
72441,7	25.84	18.79	12.00	4.01	11.02	8.37	8.55	–	3.67	2.76	1.01	84.02

Note: Table from Heiken et al. [4].

72441,7, 71.66% of particles were below 150 μm in size, with 24.36% were greater than 150 μm. At both sites, over 50% of the material sampled was greater than 212 μm particle size. At both of the sample sites, there is a greater proportion of higher quality raw regolith from which to produce the higher strength, 1.44% porosity sintered material.

Part of premise for using sintered lunar regolith as a structural material is that there will be plentiful amounts of lunar regolith to harvest and process. A problem could arise if structures to be built using ISRU lunar regolith need to be constructed in regions deprived of, or with a minimum of, regolith. Nickerson et al. [34] and Bart et al. [35] calculated regolith depths across the lunar surface. Using 143 different images from the Lunar Reconnaissance Orbiter Camera (LROC) and the Narrow Angle Camera (NAC) on LRO, regolith depth estimates were made. The maximum image size from LRO imagery is 2.5 × 26 km and it is possible to resolve meter-level detail. From these calculations, the median regolith depth in each region imaged ranges from 2.5 m to 8.7 m in depth. The shallowest lunar regolith depth occurs on the Moon's nearside maria. The Moon's far side and higher latitude regions showed the deepest lunar regolith.

The Apollo 17 landing site was at the Taurus-Littrow Valley on the eastern edge of Mare Serenitatis. This location was not directly measured for regolith depth by Nickerson et al. [33] or Bart et al. [34] but can be inferred by interpolation from their data. Using the known location of the Apollo 17 landing site, the regolith depth could be around 4–5 m. Combined with the previously discussed knowledge that regolith grain size in this region is favorable for producing 1.44% porosity sintered material, ample high quality sintered lunar regolith could be expected to be produced at this site. Alternative locations would of course need to be evaluated further for regolith grain size and regolith depth to be able to reach the same conclusion.

Table 11 shows the raw compressive strength data.

4.1.5. Compressive strength as a function of porosity

A comparison was made related to the sample density and the compressive strength of the material. The density was measured from the calculated cylindrical volume of the sample and the measured mass. Fig. 9 shows the two porosity sets compared to the compressive strength reached by the samples. As expected for the two different porosity sets, two different density sets become apparent. The higher density material, 1.44% porosity samples all obtained higher compressive strengths and similar sample densities. The lower density 11.78% porosity material had a wider range of density variation and compressive strengths.

4.1.6. Bulk modulus

One of the fundamental elastic moduli is the compression modulus, or bulk modulus, which is critical for evaluating a material's compressive loading capacity. The bulk modulus is the ratio of applied pressure to volumetric strain,

$$K = -\frac{P}{\varepsilon_V} \tag{2}$$

with results for our samples found in Table 12.

The bulk modulus numbers presented here assume an unchanging diameter during testing from the initial diameter measurements. Hence, the change in volume is only based on the change in height of the cylindrical specimen. The compression tests conducted were unconfined tests, and thus the specimen is expected to exhibit a lower bulk modulus than if tested under confined conditions. If the value of the diameter increases appreciably, failure may occur sooner.

4.1.7. Comparison to similar research

Gualtieri and Bandyopadhyay [18] provided the samples used in this testing. Similar compression testing was performed on their samples as was performed in this research. One difference between the two testing series were the porosities of the samples tested, ours were 1.44% and 11.78% where theirs were 0.41% and 8.44% porous. These additional two porosity sets allow for a refined view of the effect of porosity on compressive strength. The averaged data for both the Gualtieri [18] and the Indyk [31] compression testing can be seen in Table 13. The data is organized from 1.44% porosity to 11.78% porosity for the four sample sets tested, giving the average ultimate failure, Young's modulus and the first standard deviation.

It appears that our values for compressive strength and Young's modulus compare well with that of Gualtieri and Bandyopadhyay [18]. Important for direct comparisons, but unstated [18], was the quantity of samples tested or whether poor performing samples were discarded. Gualtieri and Bandyopadhyay may have implemented a more rigorous quality control on the samples tested than in the samples tested here. However, inspecting the first standard deviation for the 'Ultimate Failure' column in Table 13, there appears to be a similar range of maximum compressive strengths for the two independent compression tests. This points to similar variability of maximum compression strengths from both series of sintered lunar simulant testing. In the testing by Gualtieri and Bandyopadhyay [18], no premature compression failures were reported; this is noteworthy as our testing experienced a prevalence of initial failure in our samples.

It is unclear if any of the samples tested by Gualtieri and Bandyopadhyay [18] experienced initial failure. The 1.44% porous samples without initial failure (n = 3) from exceeded the ultimate failure value for the 0.41% porosity samples, but the 11.78% porosity samples were not stronger than the 8.44% samples. The reason the 1.44% porosity samples that did not experience initial failures performed better than the 0.41% porosity samples is most likely due to the range on standard deviation for both sets. The decreasing strength trend from 1.44% porosity to 11.78% porosity agrees with findings presented earlier.

We are pleased with the comparisons, and even though the tests have similar aims, we have pursued this research to provide a more extensive

Table 11
Compressive strengths for all tests.

1.44% Porosity			11.78% Porosity		
Test Number	Initial Failure (MPa)	Ultimate Failure (MPa)	Test Number	Initial Failure (MPa)	Ultimate Failure (MPa)
1	–	250.6	8	28.0	86.5
2	194.9	199.	9	–	93.0
3	–	226.4	10	27.0	35.6
4	142.0	188.0	11	136.2	138.9
5	190.3	241.1	12	–	93.6
6	–	234.6	13	–	115.6
7	145.9	191.9	14	77.3	113.9
			15	39.9	42.4
			16	31.2	41.7
Mean	197.8	218.8	Mean	71.3	84.6
STD	39.3	23.5	STD	38.9	34.9

Note: STD = standard deviation.

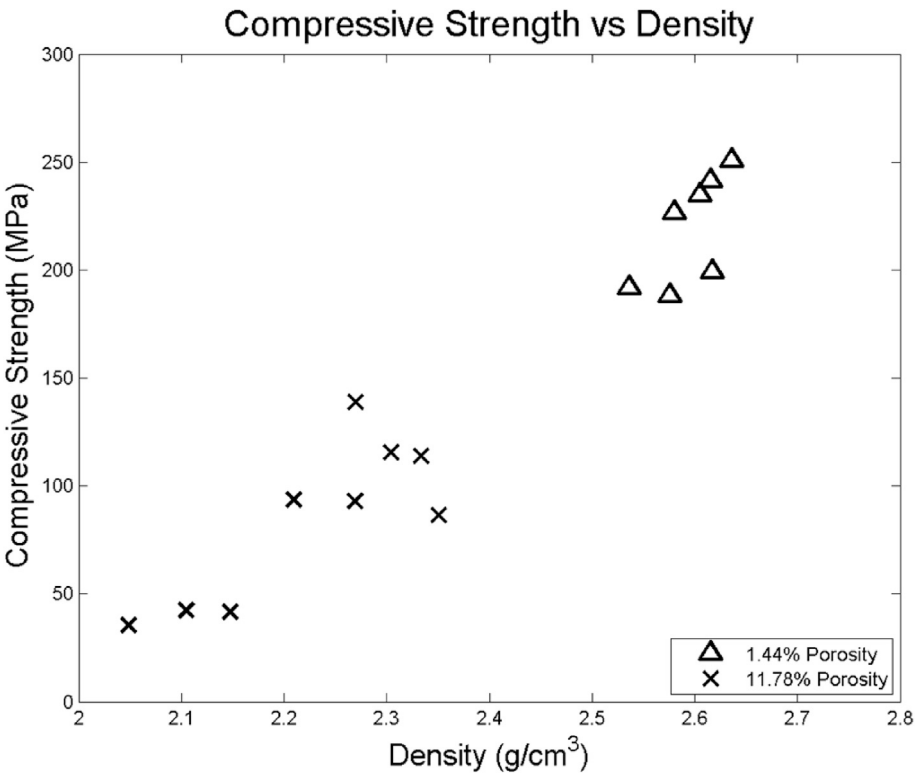

Fig. 9. Compressive strength vs. density.

discussion and data for structural designers who one day may consider using regolith as a primary building material.

5. Application of data

Our goal for the data collected and analyzed is potentially for the purpose of design of a lunar structure or other infrastructure, such as roadways, utilizing regolith in a simple way. Table 14 summarizes our results for the low and 11.78% porosity simulant samples that can be used in preliminary structural designs. Comparing alternative ISRU materials would be an important step for structural material selection. Table 15 shows compressive strength values for five simulated lunar materials from our literature review. Three compressive strength ranges for the materials can be identified that also share similar manufacturing techniques. There appear to be a low middle and high range of

Table 12
Bulk modulus.

Porosity Data Set	Failure Type	Mean (MPa)	STD	COV
1.44% (n = 8)	Initial	6389.5	1776	0.278
1.44% (n = 8)	Ultimate	5961.0	1693	0.284
11.78% (n = 8)	Initial	3659.7	2031	0.555
11.78% (n = 8)	Ultimate	3586.4	2062	0.575
1.44% (n = 3)	Ultimate	6919.0	979	0.141
11.78% (n = 3)	Ultimate	4272.0	621	0.145

Note: n = sample size, STD = standard deviation, COV = coefficient of variation.

Table 13
Comparison of sintered lunar simulant measured properties.

Mean of Porosity Data Set	Porosity (%)	Ultimate Failure (MPa)	Ultimate Failure (MPa)	E (GPa)
Low Porosity (n > 10) [18]	0.41	232.0 ± 43.7	–	10.9 ± 1.89
Low Porosity (n = 8) [31]	1.44	218.8 ± 23.5	237.2 ± 10[a]	8.4
High Porosity (n > 10) [18]	8.44	103.2 ± 26.7	–	5.98 ± 0.71
High Porosity (n = 8) [31]	11.78	84.6 ± 34.9	100.7 ± 10.5[a]	5.5

Note: n = sample size.
[a] n = 3.

Table 14
Summary of the experimental sintered samples material properties.

Material Properties at Ultimate Failure	1.44% Porosity (n = 8)		11.78% Porosity (n = 8)		Units
	Mean	STD	Mean	STD	
Compressive Strength	218.8	23.5	84.5	34.8	MPa
Bulk Modulus	5961.0	1692.8	3586.4	2061.6	MPa
Elastic Modulus	8358[a]	748	5475[b]	782	MPa
Torsion Modulus	3300	–	2198.	–	MPa
Average Density[c]	2.6	0.1	2.2	0.1	g/cm^3

Note: n = sample size, STD = standard deviation, COV = coefficient of variation.
[a] n = 6.
[b] n = 5.
[c] From unloaded measurement.

Table 15
Measured compressive strengths for various lunar resource derived structural materials.

Material	Compressive Strength (MPa)
Geothermite, simulant & aluminum[a]	10–18
Additive manufacturing, simulant & binding agent[b]	20
Lunar sulfur concrete[c]	31
Lunar concrete[d]	74
Sintered lunar simulant[e]	203–232
Sintered lunar simulant[f]	101–237

[a] Faierson et al. [13].
[b] Cesaretti et al. [16].
[c] Toutanji et al. [2].
[d] Lin [1].
[e] Gualtier and Bandyopadhyay [18].
[f] Indyk [31].

compressive strength values. On low side are the geothermite and the additive manufactured with binding agent simulants with compressive strengths of about 20 MPa. In the midrange are the lunar concretes. The upper end includes two simulants with an order of magnitude greater compressive strength. It is noteworthy that the sintered lunar simulants in Table 15 were produced by the same process and independently compression tested. The porosity of the sintered lunar simulant can be used to adjust its compressive strength.

Even without increased quality control or refined manufacturing, lower grade 11.78% porosity sintered lunar regolith is expected to be stronger than geothermic or concrete based lunar structural materials.

One material of lunar structural importance that is omitted from the above table is cast basalt. Cast basalt was first suggested as a potential lunar structural material by Happel et al. [19] and has been advocated by Benaroya et al. [6,36] as a main component of an ISRU based lunar structure. Happel et al. [19] used the assumed cast basalt properties of ultimate compressive strength of 538 MPa (78,000 psi) for his calculations. In the literature review, we could not find testing of cast basalt for ISRU structural material. However promising cast basalt is with a compressive strength in excess of twice the tested sintered lunar simulant, additional work should be performed to confirm its plausibility in the lunar environment and for verification of its material strength. One lunar effect not accounted for in our testing is the reduced lunar gravity. From what is known about sintering in microgravity or reduced gravity, greater levels of distortion of the product can be expected. The specifics of controlling this distortion through forms or finishing work in reduced gravity are yet to be investigated.

Aside from the fundamental material properties, fabrication processes need to be considered as well. Reducing initial and post processing time and equipment would be greatly beneficial to making a certain material more attractive for use. All the materials discussed here depend on extracting the lunar regolith from the surface, so excavating equipment will be required regardless of lunar regolith derived ISRU. *Utilizing the regolith in its raw form has the advantage of not requiring refining of the raw minerals out of the regolith. Refining would require additional equipment for this additional step which increases transportation costs from the Earth to the Moon, as well as increase the complexity of manufacturing construction material on the Moon, leading to an increases in the chance of mechanical malfunction and down time.*

5.1. Application to lunar structures

Lunar development would be implemented in three major phases as outlined by Happel et al. [19], Benaroya et al. [36] and Cohen [37]. The first phase would consist of transporting prefabricated modules from Earth and assembling them on the Moon over multiple missions. Phase two would allow for a marriage of terrestrial and lunar fabricated components and modules requiring assembly on the lunar surface. Finally, phase three structures would be comprised significantly of lunar ISRU structural materials. Of course, no specific ISRU based structural material has been selected for the final two phases because of the limited practical understanding of lunar materials that would need to be developed during phases one and two development. This is in part because the technology is not mature enough to make educated decisions on the optimal ISRU manufacturing process. An evaluation period of testing an ISRU manufacturing process and developing structural material could take place during phase one and phase two of lunar development, allowing for actual structural ISRU based material to be ready for phase three. This is regardless of how much terrestrial based lunar simulant testing is performed. Results presented in this research work suggest sintered lunar regolith should warrant early investigation for manufacturing on the lunar surface, possibly during the first phase of establishing a lunar presence.

Deciding which applications may be suitable for an ISRU structural material requires additional consideration. Structural design for the lunar surface is a complex process that depends on many factors. In particular are the 1/6th Earth gravity, required internal pressurization for habitability, temperature gradients, radiation shielding, micrometeorite impacts and the effects of lunar dust. Static loading conditions would have the benefit of the reduced lunar gravity. All of these factors can greatly affect the expected and unexpected loading conditions that the structure would need to endure. Cements and ceramics are strongest under compressive loads and weaker for tensile loading in comparison to other structural materials, such as metals. Terrestrially, structures that are in compression last the longest, but structures in tension are the most efficient. Specific structural members for a phase two or phase three lunar habitat would need to be evaluated on individual merits if sintered lunar regolith would be appropriate. The compressive strength values measured for sintered lunar simulant suggest that sintering actual lunar regolith could form material suitable for very high compressive loads. Offering additional versatility, if a less strong material is desired, this can be accommodated by adjusting the porosity of the sintered lunar regolith. Some examples of structures that are required to handle high compressive loading include static structures that are used for the following: load bearing members, road surfaces, dust mitigation, or launch and landing pads. Terrestrial building and construction codes govern the quality and acceptable methods of constructing these types of structures. Ettouney and Benaroya [38] initiated the discussion on lunar codes, but no lunar building and construction standards yet exist.

From solely a material strength perspective, a tiered hierarchy can be envisioned where low, medium and high grades of lunar materials are selected for varying demand uses. Geothermic structural lunar material could be at the low end of the scale for applications requiring lower strength. Sintered lunar materials could occupy the high end, satisfying the needs of higher strength applications. If sintered lunar regolith were to prove to be the best all-around material from strength and manufacturing perspectives, then it very well could be the sole material derived from ISRU resources.

Not all structural applications will depend on the strength of the material. Operating in the lunar environment is difficult and demanding. Manufacturing processes will need to be optimized to use the available resources and consumables sparingly and efficiently.

A novel method of excavating lunar regolith has been proposed by Zacny et al. [39], where a nozzle is inserted into lunar regolith and injects a gas. This gas then disperses outward due to the vacuum and kicks out the surrounding regolith. A similar method could be implemented to remove the non-sintered lunar regolith, gaining access to the now sintered component.

6. Conclusions

Sixteen manufactured sintered samples of two different porosities created for this research underwent compression testing. The loads and deflections were recorded and the effect of porosity on the modulus of elasticity and bulk modulus were calculated.

Sintering lunar regolith simulant produces a structurally strong material that can be used as an analogue to what could be formed on the lunar surface with actual lunar regolith.

One difficulty was the initial failures that occurred during some of the tests and how to handle the data from those tests. It is believed that by refining the manufacturing quality control and the testing process of the samples of sintered lunar regolith, these premature failures could be greatly reduced. However, even using the initial failure data sets demonstrated impressively strong compressive strengths. In comparison to other terrestrial concretes and lunar structural materials, sintered lunar simulant proved to have the highest experimentally tested compressive strength. This bodes well for comparable sintered lunar regolith that is expected to be similar if not stronger on the Moon since the lunar environment provides better conditions for the sintering process.

We expect that on the Moon, very strong 1.44% porosity sintered material is ubiquitous due to the effects of constant meteor

bombardment. Future work should evaluate whether un-sieved lunar simulant could produce usable and reliable samples with high compressive strengths, thus not requiring the separation used in this work where two categories of simulant sizes were created.

There is value in continuing what we started here, evaluating how well "poor quality" regolith can satisfy structural needs. We note that even the worst performing 1.44% porosity sample performed better than the average 11.78% porosity sample set. And even though the material may be brittle, it can hold high compressive loads even after fracture.

For equal comparisons across various lunar materials, a standard for testing lunar samples should be created to ensure accurate comparisons. Better testing criteria are also needed. The terrestrial equivalents can be found in standards such as ASTM C39 'Standard Test Method for Compressive Strength of Cylindrical Concrete Specimens.' Lunar materials could have standards fashioned in a similar format.

Further knowledge could be gained about sintered lunar regolith if reinforcement can be added during the fabrication process. With steel reinforcement, similar to reinforced concrete, tension loads would be handled much better, lending greater flexibility to structural member usage. Regolith brittleness will need to be countered.

A complete design of a lunar structure using the material properties of the sintered lunar simulant presented here would be interesting. This would provide a better understanding of how much lunar regolith would be needed to construct a usable structure, providing criteria for excavation and manufacturing equipment needed to process and form the regolith into sintered material. An excellent starting point for such a structural design would be the structure in the work by Ruess et al. [22].

Impact resistance of porous material could be valuable and studied further. Though not investigated in this research, the ability of porous sintered regolith to absorb micrometeorite impacts should be promising. During the 1702 siege of Fort Castillo De San Marcos in St. Augustine, Florida by English warships, the stone used to construct the fort was credited with saving it. This stone is called the coquina, similar to limestone but comprised of ancient seashells that had bonded together and is full of voids. It allowed the cannon balls to be cushioned and softened the impact, subsequently minimizing any cannonball damage. *Micrometeorite impacts could be mitigated or better controlled by a similar porous outer structural layer. This outer layer could be comprised of an 11.78% porosity sintered lunar regolith.* If sintered lunar regolith proves to be useful for micrometeorite shielding, it could be envisioned that its use could replace mounds of raw lunar regolith on top of lunar structures for shielding. This could be one more suitable application of this new material.

Funding

This research did not receive any specific grant from funding agencies in the public, commercial, or not-for-profit sectors.

Acknowledgements

We are grateful to Professor Amit Bandyopadhyay and his student Thomas Gualtieri of Washington State University for creating samples using JSC-1A simulant donated by Honeybee Robotics. Joe Vanderveer, John Petroski and Terence Whalen of Rutgers University all played important roles in assisting with setting up the equipment used to test the material samples. From the Caltech Jet Propulsion Laboratory, Ashley Chandler, Mark Balzer and Lori Shiraishi all offered their time and assistance with the testing of the material samples.

References

[1] T.D. Lin, H. Love, D. Stark, Physical properties of concrete made with Apollo 16 lunar soil sample, in: American Institute of Aeronautics and Astronautics, Proceedings, October 1987, 1987.
[2] H. Toutanji, S. Evans, R. Grugel, Performance of lunar sulfur concrete in lunar environments, Constr. Build. Mater. 29 (2012) 444–448.
[3] L.A. Taylor, T.T. Meek, Microwave sintering of lunar soil: properties, theory, and practice, J. Aerosp. Eng. 18 (2005) 188–196.
[4] G. Heiken, D. Vaniman, B. French, Lunar Sourcebook: a User's Guide to the Moon, Cambridge Univ. Press, Cambridge, 1991.
[5] M.B. Duke, L.R. Gaddis, G.J. Taylor, H.H. Schmitt, Development of the Moon, Rev. Mineral. Geochem. 60 (2006) 597–656.
[6] H. Benaroya, L. Bernold, Engineering of lunar bases, Acta Astronaut. 62 (2008) 277–299.
[7] H. Benaroya, Phil Metzger, Anthony Muscatello, Editors, (2013) ISRU for Extraterrestrial Construction, Special Issue ASCE J. Aerosp. Eng., vol. 26, No. 1.
[8] H. Benaroya, S. Indyk, S. Mottaghi, Advanced systems concept for autonomous construction and self-repair of lunar surface ISRU structures, in: V. Badescu (Ed.), Moon Prospective Energy and Material Resources, Springer, Berlin, 2012, pp. 641–660.
[9] G.A. Landis, Materials refining on the Moon, Acta Astronaut. 60 (2007) 906–915.
[10] H. Benaroya, S. Mottaghi, Z. Porter, Magnesium as an ISRU-derived resource for lunar structures, J. Aerosp. Eng. (2012) 152–159.
[11] C.C. Allen, J.C. Graf, D.S. McKay, Sintering bricks on the Moon, in: R.G. Galloway, S. Lokaj (Eds.), Proceedings of the ASCE Specialty Conference (Space'94), Albuquerque, NM, 26 February-3 March, ASCE, New York, NY, 1994, pp. 1220–1229.
[12] Hung, C-C. and McNatt, J. (24 Feb, 2010). Lunar dust simulant containing nanophase iron and method for making the same. Patent 20110204185A1.
[13] E. Faierson, K. Logan, B. Stewart, M. Hunt, Demonstration of concept for fabrication of lunar physical assets utilizing lunar regolith simulant and a geothermite reaction, Acta Astronaut. 67 (2010) 38–45.
[14] M.A. Hobosyan, K.S. Marturosyan, Sintering of regolith by activated thermites: a novel approach for lunar in situ resource utilization, in: 43ed Lunar and Planetary Science Conference, 2012.
[15] V. Balla, L. Roberson, G. Connor, S. Trigwell, S. Bose, A. Bandyopadhyay, First demonstration on direct laser fabrication of lunar regolith parts, Rapid Prototyp. J. 18 (2012) 451–457.
[16] G. Cesaretti, E. Dini, X. De Kestelier, V. Colla, Building components for an outpost on the lunar soil by means of a novel 3D printing technology, Acta Astronaut. 93 (2014) 430–450.
[17] E.H. Cardiff, B.C. Hall, A dust mitigation vehicle utilizing direct solar heating, in: Joint Annual Meeting of LEAG-IECUM-SRR, October 28–31, 2008, 2008.
[18] T. Gualtieri, A. Bandyopadhyay, Compressive deformation of porous lunar regolith, Mater. Lett. 143 (2015) 276–278.
[19] J.A. Happel, K. Willam, B. Shing, Prototype lunar base constructing using indigenous materials, SPAE 92 engineering, construction, and operations in space, Proc. ASCE, New York (1992) 112–122.
[20] C. McLemore, J. Fikes, K. McCarley, J.E. Good, S.D. Gilley, J.P. Kennedy, From Lunar Regolith to Fabricated Parts: Technology Developments and the Utilization of Moon Dirt, 2008. Retrieved July 21, 2015, from http://ntrs.nasa.gov/search.jsp?R=20080018923.
[21] C.S. Ray, S.T. Reis, S. Sen, J.S. O'Dell, JSC-1A lunar soil simulant: characterization, glass formation, and selected glass properties, J. Non-Crystalline Solids (2010) 2369–2374.
[22] F. Ruess, J. Schaenzlin, H. Benaroya, Structural design of a Lunar habitat, J. Aerosp. Eng. 19 (3) (2006).
[23] T.L. Wilson, K.B. Wilson, Regolith sintering a solution to lunar dust mitigation, Lunar and Planetary Science XXXVI (2005).
[24] P. Hintze, J. Curran, T. Back, Lunar surface stabilization via sintering or the use of heat cured polymers, in: 47th AIAA Aerospace Sciences Meetings Including the New Horizons Forum and Aerospace Exposition, 2009.
[25] R.M. German, Sintering Theory and Practice, Wiley, New York, 1996.
[26] A. Upadhyaya, R. German, Gravitational effects during liquid phase sintering, Mater. Chem. Phys. 67 (2001) 25–31.
[27] R.M. German, Gravitational Effects on Liquid Phase Sintering - Distortion Observations, Unpublished manuscript. Retrieved from:, 2003 https://www.cavs.msstate.edu/publications/docs/2003/07/2003-17.pdf.
[28] S.J. Park, S.H. Chung, J.L. Johnson, R.M. German, Distortion Simulation of Liquid Phase Sintering on Earth on the Moon and Mars and in Space, Metal Powder Industries Federation, 2006.
[29] Marshal Space Flight Center, Unpublished source, in: In situ resource utilization (ISRU) element, 2010, http://isru.msfc.nasa.gov/lib/Documents/Simulant-listing.pdf.
[30] D. Rickman, J. Edmunson, C. McLemore, Functional comparison of lunar regoliths and their simulants, J. Aerosp. Eng. 26 (2013) 176–182.
[31] S.J. Indyk, Structural Members Produced from Unrefined Lunar Regolith, A Structural Assessment, Masters Thesis, Department of Mechanical and Aerospace Engineering, Rutgers University, October 2015.
[32] National Ready Mixed Concrete Association, What, Why & How? Testing Compressive Strength of Concrete, Concrete in Practice, 2003.
[33] E. Bridgford, A. Eustes, Physical Properties of Basalt, Ice, and Permafrost Report in Support of the Martian Subsurface Explorer, Colorado School of Mines, 1999. JPL Contract #961494.
[34] R.D. Nickerson, G.D. Bart, T. Lawder, H.J. Melosh, Global lunar regolith depths revealed, in: Lunar Planetary Science Conference 2011, 2011.
[35] G. Bart, R. Nickerson, M. Lawder, H. Melosh, Global survey of lunar regolith depths from LROC images, Icarus (2011) 485–490.
[36] H. Benaroya, L. Bernold, K.M. Chua, Engineering, design, and construction of lunar bases, J. Aerosp. Eng. 15 (2) (2002) 33–45.

[37] M.M. Cohen, Selected Precepts in Lunar Architecture. Tech. Rep., 53rd Int. Astronautical Congress, The World Space Congress, Houston, 2002.
[38] M. Ettouney, H. Benaroya, Regolith mechanics, dynamics, and foundations, J. Aerosp. Eng. (1992) 214–229.
[39] K. Zacny, J. Craft, M. Hedlund, P. Chu, G. Galloway, R. Muller, Investigating the efficiency of pneumatic transfer of JSC-1A lunar regolith simulant in vacuum and lunar gravity during parabolic flights, in: AIAA SPACE 2010 Conference and Exposition, 2010.

fx1Stephen Indyk is a senior project engineer and flight operations team lead for Honeybee Robotics. He is a science team member for both the Mars Science Laboratory (MSL), Curiosity rover and the Mars Exploration Rover (MER), Opportunity. As such he operates both the Rock Abrasion Tool (RAT) and the Sample Analysis on Mars (SAM) instruments. Stephen received both his M.S. and B.S. from Rutgers University in mechanical engineering. His research interests include mechanisms and technologies for in-situ resource utilization as well as sample acquisition systems.

fx2Haym Benaroya is a Professor of Mechanical and Aerospace Engineering at Rutgers University. His research interests are focused on the conceptualization and analysis of structures placed in challenging environments. These include offshore drilling structures and lunar surface structures for manned habitation. Professor Benaroya earned his BE degree from The Cooper Union in New York, and his MS and PhD from the University of Pennsylvania in Philadelphia. Prior to joining Rutgers University in 1989, Professor Benaroya was a senior research engineer at Weidlinger Associates in New York for eight years. While at Rutgers, Professor Benaroya has mentored twelve students to their PhDs and a similar number to their MS degrees. He is the author of about 80 refereed journal publications, two text books - one in Vibration and the other in Probabilistic Modeling - and two research monographs with two former PhD students on structural dynamics in the ocean. His book, “From Dust to Gold - Building a Future on the Moon and Mars,” presents a vision of settling the solar system. It was the 2012 Best Engineering Sciences Book by the International Academy of Astronautics. Professor Benaroya is an elected member of the International Academy of Astronautics.